**PR12-17-008**

Proposal to Jefferson Lab PAC 45

# Polarization Observables in Wide-Angle Compton Scattering at large $s$, $t$, and $u$

G. Niculescu (co-spokesperson) and I. Niculescu
*James Madison University, Harrisonburg, VA 22807*

B. Wojtsekhowski (co-spokesperson), A. Camsonne, P. Degtiarenko, R. Ent, D. Gaskell, D. Higinbotham, M. Jones, C. Keith, C. Keppel, D. Mack, R. Michaels, B. Sawatzky and S.A. Wood
*Thomas Jefferson National Accelerator Facility, Newport News, VA 23606*

D. Day (co-spokesperson), D. Keller (co-spokesperson), J. Zhang (co-spokesperson), G. Cates, D. Crabb, R. Lindgren, N. Liyanage, V. Nelyubin, D. Perera and M. Yurov
*University of Virginia, Charlottesville, VA 22901*

D.J. Hamilton (spokesperson-contact), J.R.M. Annand, D.G. Ireland, K. Hamilton and R.A. Montgomery
*University of Glasgow, Glasgow G12 8QQ, UK*

S. Ali, M. Carmignotto, T. Horn, G. Kalicy, A. Mkrtchyan, R. Trotta and A. Vargas
*The Catholic University of America, Washington, DC 20064*

A. Asaturyan, A. Mkrtchyan, H. Mkrtchyan, V. Tadevosyan, A. Shahinyan, H. Voskanyan and S. Zhamkochyan
*A.I. Alikhanyan National Science Laboratory, Yerevan 0036, Armenia*

E. Cisbani, M. Capogni, A. Del Dotto, F. Garibaldi and S. Frullani
*INFN Rome gruppo collegato Sanita and Instituto Superiore di Sanita, Rome, Italy*

G. Salmé and G. M. Urciuoli
*INFN Rome and La Sapienza University, Rome, Italy*

V. Bellini, F. Mammoliti and C.M. Sutera
*INFN Catania and University of Catania, Catania, Italy*

G.B. Franklin and B. Quinn
*Carnegie Mellon University, Pittsburgh, PA 15213*

A.J.R. Puckett and F. Obrecht
*University of Connecticut, Storrs, CT 06269*

A. Ahmidouch and S. Danagoulian
*North Carolina A&T State University, Greensboro, NC 27411*

C. Fanelli
*Masachusetts Institute of Technology, Cambridge, MA 02139*

E.J. Brash and P. Monaghan
*Christopher Newport University, Newport News, VA 23606*

C. Hyde
*Old Dominion University, Norfolk, VA 23529*

The Neutral Particle Spectrometer collaboration:
`https://wiki.jlab.org/cuawiki/index.php/Collaboration`

May 22, 2017

## NEUTRAL PARTICLE SPECTROMETER (NPS) COLLABORATION


A. Camsonne, R. Ent, C. Keppel, S.A. Wood, B. Wojtsekhowski, C. Zorn
*Jefferson Lab, Newport News, Virginia 23606*

A. Asaturyan, H. Mkrtchyan, V. Tadevosyan,
S. Zhamkochyan
*A.I. Alikhanyan National Science Laboratory, Yerevan 0036, Armenia*

M. Guidal, C. Munoz-Camacho
*Institut de Physique Nucleaire d'Orsay, IN2P3, BP 1, 91406 Orsay, France*

S. Ali, M. Carmignotto, T. Horn
G. Kalicy, A. Mkrtchyan, R. Trotta, A. Vargas
*The Catholic University of America, Washington, DC 20064*

C. Hyde, M.N.H. Rashad
*Old Dominion University, Norfolk, Virginia 23529*

P. King, J. Roche
*Ohio University, Athens, Ohio 45701*

D. Day, D. Keller, D. Perera, O. Rondon, J. Zhang
*University of Virginia, Charlottesville, Virginia 22904*

J.R.M. Annand, D.J. Hamilton
*University of Glasgow, Glasgow, Scotland, UK*

S. Sirca
*University of Ljubljana, Ljubljana, Slovenia*

D. Dutta
*Mississippi State University, Starkville, MS 39762*

E. Kinney
*University of Colorado, Boulder, CO 80309*

I. Albayrak
*Akdeniz University, Turkey*

P. Nadel-Turoński
*Stonybrook University, Stonybrook, NY 11794*

K.-T. Brinkmann, S. Diehl, R. Novotny, H.-G. Zaunick
*Giessen University, Giessen, Germany*

M. Boer
*Los Alamos National Laboratory, Los Alamos, NM 87545*

V. Bellini
*University of Catania, Catania, Italy*

I. Strakovsky
*George Washington University, Washington, DC 20052*

G. Niculescu
*James Madison University, Harrisonburg, Virginia 22807*

R. Paremuzyan
*University of New Hampshire, Durham, New Hampshire 03824*

# Contents

**Abstract**

An experiment is proposed to measure the initial-state helicity correlation observables $A_{LL}$ and $A_{LS}$ in Wide-Angle Compton Scattering (WACS) with a circularly polarized photon beam incident on a polarized proton target at invariant $s$ in the range of 9 to 20 GeV$^2$ and scattering angles of $\theta_p^{\rm cm} = 70^\circ$, $90^\circ$ and $110^\circ$.

Two previous JLab experiments, E99-114 and E07-002, demonstrated the feasibility of experimental real Compton scattering using a very high intensity untagged photon beam mixed with an electron beam. These experiments provided high precision results for the differential cross section and polarization transfer observables, admittedly at relatively low values of $-t$ or $-u$ for the latter. The recent E07-002 result for $K_{LL}$ was intriguing and unexpected, as it was found to be three times larger than predicted by the GPD-based model at $\theta_p^{\rm cm} = 70^\circ$. One possible way to reconcile this result with the GPD-based prediction is adjustment of the axial GPD $\tilde{H}$, which defines the $R_A$ form factor of WACS to which $K_{LL}$ is sensitive. If confirmed, such a conclusion would have a significant impact in several research fields where the nucleon's axial current is important. Furthermore, measurement of $A_{LS}$ will provide constraints on the poorly understood GPD $E$ and the role of quark orbital angular momentum at high momentum transfer. The WACS polarization observable results motivate this proposed study at significantly higher $s$ than was done (or proposed) previously, and with much higher precision. One difficulty is that the previous published experimental results, especially at $\theta_p^{\rm cm} = 120^\circ$, are in a kinematic regime where applicability of a factorized reaction mechanism can be called into question. This will unambiguously not be the case for the proposed measurements.

The increase in beam energy made possible by the recently completed upgrade of the CEBAF accelerator leads to a significant loss of counting rate due to much lower cross sections compared to previous WACS experiments. This therefore requires a novel approach with high incident photon flux and large solid angle detectors. The proposed experiment will utilize an untagged bremsstrahlung photon beam and a polarized ammonia target. An intense pure photon beam will be produced from a 10% radiator at a distance of 2 m from the target and separated from the post-radiator electron beam by employing a novel hermetic magnet-dump. The scattered photon will be detected in the high resolution Neutral Particle Spectrometer (NPS), while the coincident recoil proton will be detected in the BigBite spectrometer, which offers both large solid angle and momentum acceptance. This represents a complete redesign of the experimental setup and results in a significantly improved figure-of-merit compared with previous measurements.

Measurement of $A_{LL}$ and $A_{LS}$ to a statistical precision of 10% or better over a broad range of $s$ and $-t$ will provide stringent tests of the WACS reaction mechanism and constrain $\tilde{H}$ and $E$ at high $-t$. We therefore propose measurements at six carefully chosen kinematic settings in Hall C, for which we request 1100 hours with electron beam energies of 8.8 GeV and 11 GeV.

# 1 Introduction

As several proposals with similar physics goals have been submitted to the Jefferson Lab PAC over the years, this section presents a brief overview of the experiments on Compton scattering from the proton in the wide-angle regime and outlines the key aspects of the experimental technique that has been adopted for the current proposal at high $s$, $-t$ and $-u$.

## 1.1 Experiments at CEA and Cornell

In the early 1970s several measurements of Compton scattering from the proton at photon energies of a few GeV were performed at CEA and Cornell. The first experiment in the wide-angle regime with large $s$, $-t$ and $-u$ was performed at Cornell in 1977 [1]. It used a pure photon beam produced on a 10% radiator and a liquid hydrogen target. Detection of the proton in a magnetic spectrometer, and of the scattered photon in a segmented lead-glass calorimeter, allowed selection of the WACS signal in spite of 20-50 times higher rate of single pion photo-production background events. The intensity of the photon beam and resulting luminosity was limited by the counting rate in the tracking detectors of the proton arm. This rate limitation was due to the location of the tracking chamber in front of the dipole, which was required for determination of the event vertex due to the large transverse size of the photon beam spot. The Cornell experiment was highly successful and provided the first measurement of the WACS cross section in the several GeV regime. At the highest photon energy of 6 GeV, separation of WACS and background ($\pi^0$) events became less reliable due to insufficient angular resolution of the detectors, and potentially led to overestimation of the WACS cross section at the highest values of $s$ and $-t$. The most well known results of Cornell's experiment are a disagreement of experimental cross section with pQCD calculations by one to two orders of magnitude, yet agreement with pQCD on the s-scaling of the cross section.

## 1.2 First JLab 6 GeV WACS experiment

In 1994, development began on a WACS experiment at JLab for which the 100% duty factor electron beam provided a factor of 15 advantage over Cornell for the accidental rates. Development of a JLab experiment with a well shielded proton spectrometer and highly segmented calorimeter was an appealing challenge from the outset. Utilization of a pure photon beam (like Cornell) was far from trivial due to the significant shielding requirements needed to dump electrons after they pass through the radiator. Many photon beam experiments, especially at SLAC, were performed with a mixed electron-photon beam and a radiator in/out method. The same method was used in high energy deuteron photo-disintegration measurements [2]. This approach not only eliminates the need for construction of a local beam dump but also allows a compact photon beam spot size at the target which improves angular reconstruction of the $\gamma$-p events. However, for Compton scattering the mixed beam

has never been used because the two-body angular correlation – the key method of event reconstruction – does not distinguish $\gamma$-p from elastic electron-proton scattering which has a much higher rate.

A Letter of Intent (LOI 95-003) was submitted to PAC10 in 1995, followed by a full proposal (PR97-108) in 1997 [3], which considered several options for running with a mixed beam, such as a highly segmented array of scintillator counters for tagging of an electron scattered from a proton. In addition, the energy of the incident photon was proposed to be significantly below the end point where most of the e-p events are concentrated. The possibility of constructing a chicane for electron beam transport around the target to the main beam dump was also considered. Finally, a deflection magnet between the target and the photon detector was proposed as a means of kinematic separation of the electron and photon scattering events.

Around that time, development of the GPD formalism [4] and a GPD-based calculation of the WACS cross section and polarization observables by M. Diehl and P. Kroll [5] renewed interest in the proposed physics subject. After two short tests the design of the experiment was finalized and a new proposal (PR99-114) was approved in 1999 for measurement of both the cross section and polarization transfer observable $K_{LL}$ [6]. Experiment preparation required construction of a 700-block calorimeter, 200-bar Čerenkov lucite electron tagger and a custom deflection magnet. Measurements were performed in January-February 2002, and the results demonstrated good agreement with the GPD-based predictions and striking disagreement with the pQCD two-gluon exchange mechanism [7, 8], which many physicists at the time thought provided the best description of hard exclusive reactions at JLab energies.

## 1.3 Followup 6 GeV Era Proposals and Experiments

Following the success of the E99-114 experiment a new measurement of $K_{LL}$ (E03-003) was approved and later updated (as E07-002) in order to firmly establish its $t$-dependence and obtain data in the kinematic regime where interpretation of the results in the GPD framework is more reliable [9]. The Hall C part of the E07-002 plan took data in 2008, the result of which showed unexpected disagreement with the published theoretical predictions [10]. However, recent re-analysis of the GPD-based model calculation with a modified $\tilde{H}$ function based on uncertainty on the proton's axial form factor found reasonable agreement between theory and both JLab experiments [11]. It is difficult to draw from this a definitive statement on proton structure as a result of the relatively low value of $-t$. This again underlines the importance of future measurements having sufficiently large values of all kinematic parameters.

In a 2004 paper Miller suggested that the initial-state helicity correlation $A_{LL}$ is not equal to its final-state equivalent ($K_{LL}$) because the helicity-flip amplitude is not suppressed when scattering occurs from a heavy object like a constituent quark [12]. This motivated the development of another proposal (approved as E05-101) to measure $A_{LL}$ by using a mixed electron-photon beam and a polarized hydrogen target in Hall C, with the HMS as a proton spectrometer [13]. Although the proposal was approved by PAC28 with an A- rating the

experiment was not scheduled before shutdown for the 12 GeV upgrade.

## 1.4 12 GeV Era Proposals

Upgrade of the CEBAF accelerator opens up a new window on the high $-t$ physics to which WACS is uniquely sensitive, as presented in the 12 GeV plan. The first priority was a new differential cross section measurement, which could be performed up to $s$ of 22 GeV$^2$. These efforts were aided by the development of a high resolution calorimeter (NPS) proposed by CUA, JLab, ANSL and collaborators. An optimized set of cross section measurements utilizing the new NPS detector system was approved by PAC42 (E12-14-003) in 2014 [14].

Measurement of the polarization transfer observable $K_{LL}$ at higher energy is exceedingly time consuming because of the rapid reduction of the polarimeter figure-of-merit at high proton momenta. However, the figure-of-merit of a polarized target remains largely constant as beam energy is increased. This motivated submission of a similar proposal to E05-101 with a mixed electron-photon beam, polarized ammonia target and the NPS. This proposal was approved by PAC43 as E12-14-006 and covered a similar kinematic range to the published $K_{LL}$ results [15].

An important consideration for design of a polarized WACS experiment is that the low luminosity operation of the polarized target, limited by the target characteristics, allows the use of a large acceptance proton detector such as the Super BigBite Spectrometer (SBS) [16]. Another key consideration that has been discussed for over ten years is operation of a low temperature polarized target with a pure photon beam. This would allow much higher photon intensity due to a reduction of the heat load and radiation damage of the target induced by the electron beam. Indeed, the use of a pure photon beam would allow for an increase of photon intensity by a factor 10 to 30 [17]. Crucially, it would also eliminate the contribution to the overall systematic uncertainty from radiative elastic electron scattering events, which proved a troublesome background to handle in the 6 GeV era experiments.

There have been a number of polarized target experiments with pure photon beams produced by bremsstrahlung radiation, all of which required a powerful dipole magnet for removal of the electron beam to a beam dump. In the case of WACS, the radiator needs to be located near the target because of the necessity for a small transverse beam spot at the target. This limits the maximum radiator-to-target distance to 2 – 4 meters (depending of the electron beam energy), or requires tight collimation of the photon beam and therefore a reduction in intensity. Another complication is related to the use of a 10% radiator, which means the degraded electrons have a very wide energy distribution, making it difficult to find a suitable arrangement for a beam dump and increasing power dissipation near the target.

In 2014 at the NPS meeting, two very different concepts for a photon source were presented. Both utilized a 10% radiator, but while one design was based on the traditional scheme of a photon source with a beam dump at a large distance from the radiator [18], the other was based on the idea of complete hermeticity of the magnet/dump except for a narrow aperture for the incident electron beam and a similar aperture for the outgoing high

energy photon beam (Hermetic Compact Photon Source) [19].

A WACS proposal based on the HCPS concept (PR12-15-003) was submitted to PAC43, and planned on focusing on an $s$-scan of $A_{LL}$ at $\theta_p^{\rm cm} = 90^\circ$ with maximum $s$ of 15 GeV$^2$ [20]. This ambitious proposal represented a significant increase in the figure-of-merit relative to the plan in E05-101/E12-14-006. This was possible due to the large acceptance of the proton spectrometer and high photon intensity from the proposed HCPS. The large angular and momentum acceptance of the Super BigBite Spectrometer used for the recoil proton detection allowed simultaneous data taking over a wide range of photon energies: the s-scan in a single detector setting. The PAC43 report recommended adding a measurement at $\theta_p^{\rm cm} = 120^\circ$ and expressed strong interest in the novel concept of the photon source which provides high intensity and small size photon beam at the target.

In 2016 a new proposal, PR12-16-009, with the more traditional scheme of photon source and HMS advocated measurements of both $A_{LL}$ and $A_{LS}$ [21]. Responding to this, PAC44 made the recommendation of holding a workshop to discuss the two designs of the photon source and physics priorities. With support from JSA the NPS collaboration, this workshop took place in February 2017 at the Catholic University of America, the proceedings from which were recently published [22].

## 1.5 The Current Proposal

The current proposal arises as a result of the discussions that have been taking place for the past few years, with the collaboration converging on an optimal experimental technique following the workshop earlier this year. The basic concept involves a pure photon beam produced on a radiator 2 m from the polarized target and large acceptance photon and proton detectors. The main change compared with PR12-15-003 is the use of BigBite rather than Super BigBite for the proton spectrometer to accommodate running in Hall C. This is partly motivated by compatibility with the NPS and beam-time availability. Furthermore, as the calculations of the radiation outside of the photon source have become more advanced, they have indicated that the design is sufficiently robust to allow running with double the beam current compared to the value used in the previous proposals. This has also been made possible by the concept of target rotation for uniform illumination of the target cell.

The spokespeople have been actively engaged with the theorists working on WACS, partly as a result of a dedicated workshop on transverse nucleon structure at high momentum transfer in Trento in 2016 [23] and further discussions at the High-Intensity Photon Source workshop. Peter Kroll, who was present at both workshops, stressed the importance of making new measurements at the highest possible values of $s$, $-t$ and $-u$, in order to ensure the validity of factorization and extract meaningful information on the proton's structure [22]. We have also been engaged with the advances that have been made in the past few years on the Soft Collinear Effective Theory. The physics motivation for the current proposal has been updated accordingly, stressing the connection to other areas of physics such as neutrino scattering experiments and the proton's axial structure in light of the most recent

JLab results.

In terms of the choice of kinematic settings, in addition to the key $s$-scan at $\theta_p^{\rm cm} = 90^\circ$ that was previously proposed, two measurements with 8.8 and 11 GeV beam energies at $\theta_p^{\rm cm} = 70^\circ$ have been added, for which the rates are much higher. The request by PAC43 to add an $s$-scan of $A_{LL}$ at $\theta_p^{\rm cm} = 120^\circ$ has been carefully studied, but the combination of low $-u$, even with an 8.8 GeV beam, and very low WACS cross section at high $-t$ makes this setting prohibitively beam-time intensive. As a compromise, a setting at $\theta_p^{\rm cm} = 110^\circ$ has been added. In order to maximize the physics impact of the proposed experiments and probe the theoretical models in detail, we have added measurements of the transverse observable $A_{LS}$. Taken together with the cross sections results, the proposed measurements will represent a major step forward in our understanding of hard exclusive reactions and prove invaluable in moving the theoretical framework forward.

# 2 Physics Motivation

## 2.1 Overview

Significant progress has been made over the last decade in our understanding of exclusive reactions in the hard scattering regime. This progress had been made possible, in part, by data from Jefferson Lab on elastic electron scattering and Compton scattering from the proton, and by a significant and increasingly sophisticated theoretical effort to exploit the richness of exclusive reactions at moderate momentum transfer.

The observation of scaling in Deep Inelastic Scattering (DIS) at relatively low momentum transfers, successfully understood within the framework of pQCD, suggested that the same interpretation would apply to exclusive reactions: elastic electron scattering, photo- and electro-production of mesons, and Compton scattering. This prospect was further supported by the fact that constituent counting rules [24, 25], which naturally govern reactions that conform to the pQCD picture, could describe certain exclusive reactions. There is little doubt that the pQCD mechanism dominates at high energies, but what has been lacking is agreement on the scale at which the transition occurs. The argument on this point is driven by more than a difference of (theoretical) opinion. The unavoidable fact is that cross sections calculated in a pQCD framework have invariably been low when compared to data, sometimes by an order of magnitude or more [26, 27].

Results of experiments at Jefferson Lab on the proton contradict the predictions of pQCD: the recoil polarization measurements of $G_E^p$ E93-027, E04-108 and E99-007, and the Real Compton Scattering (RCS) experiment E99-114. The $G_E^p$ measurements found that the ratio of $F_2$ and $F_1$, scaled by $Q^2$ demands a revision of one of the precepts of pQCD, namely hadron helicity conservation [28, 29, 30]. The result from the RCS measurements that the longitudinal polarization transfer $K_{LL}$ is large and positive is also contrary to the pQCD predictions [7] . These experiments provide a compelling argument that pQCD should not be applied to exclusive processes at energy scales of 5-10 GeV.

Fortunately, an alternate theoretical framework exists for the interpretation of exclusive scattering at intermediate energies [31, 5, 32]. This alternative approach asserts the dominance of the handbag diagram in which the reaction amplitude factorizes into a sub-process involving a hard interaction with a *single quark*. The coupling of the struck quark to the spectator system is described by Generalized Parton Distributions (GPDs) [33, 34]. Since the GPDs are independent of the particular hard scattering reaction, the formalism leads to a unified description of hard exclusive reactions. Moreover, the relationship between GPDs and the normal parton distribution functions provides a natural framework for relating inclusive and exclusive reactions.

The RCS experiment E99-114 produced an especially remarkable result; not only was the measurement of $K_{LL}$ inconsistent with pQCD, it was found that the longitudinal polarization is nearly as large as that expected for scattering from a free quark. Clear overlap of this result is seen in the leading predictions using a handbag approach based on GPDs [32], Soft Collinear Effective Theory [35] and the relativistic Constituent Quark model [12]. But

what is even more remarkable is that the new $K_{LL}$ measurement from E07-002 is inconsistent with prediction from *all* of these theoretical approaches, indicating a need for further measurements [10].

In light of this, the key questions that motivate further exploration of the WACS polarization observables at JLab are:

1. To what degree is the factorized mechanism dominant at 12 GeV energies, and how significant are target mass and other higher twist corrections?

2. What are the constraints on the GPD moments imposed from the proposed measurements of the $A_{LL}$ and $A_{LS}$ observables, and what do they tell us about the proton's axial and tensor structure at high $-t$?

3. What is the nature of the quark which absorbs and emits photons in the Compton scattering process in the wide angle regime? Is it a constituent or a current quark?

4. What does a direct comparison of the SCET and GPD predictions tell us about the handbag mechanism, the non-perturbative structure to which it is sensitive and the role of hadron helicity-flip?

## 2.2 The Handbag Mechanism

The handbag framework represents the most developed approach for interpretation of hard exclusive reactions such as deeply virtual processes, characterized by high-$Q^2$ and low $-t$, and wide-angle reactions at high $-t$. The application of the formalism to WACS (see Fig. 1) in a GPD-based approach was initially worked out to leading order (LO) by Radyushkin [31] and subsequently by Diehl *et al.* [5]. The next-to-leading-order (NLO) contributions were subsequently calculated by Huang *et al.* [32]. In the handbag approach, the hard physics is contained in the scattering from a single active quark and is calculable using pQCD and QED: it is just Compton scattering from a structureless spin-1/2 particle. The soft physics is contained in the wave functions describing how the active quark couples to the proton.

## 2.3 The GPD Model

To predict the behavior of wide-angle Compton scattering a model for the GPDs at large $-t$ and zero skewedness is required, which is based on a representation in terms of light-cone wave function overlaps. This then allows modeling of the GPDs by parameterizing the transverse momentum dependence of an $N$-particle wave function respecting the central assumptions of the handbag approach necessary to achieve factorization of the amplitudes into soft and hard parts.

The GPDs have been the subject of intense experimental and theoretical activity [33, 34]. They represent superstructure of the proton, from which are derived other measurable

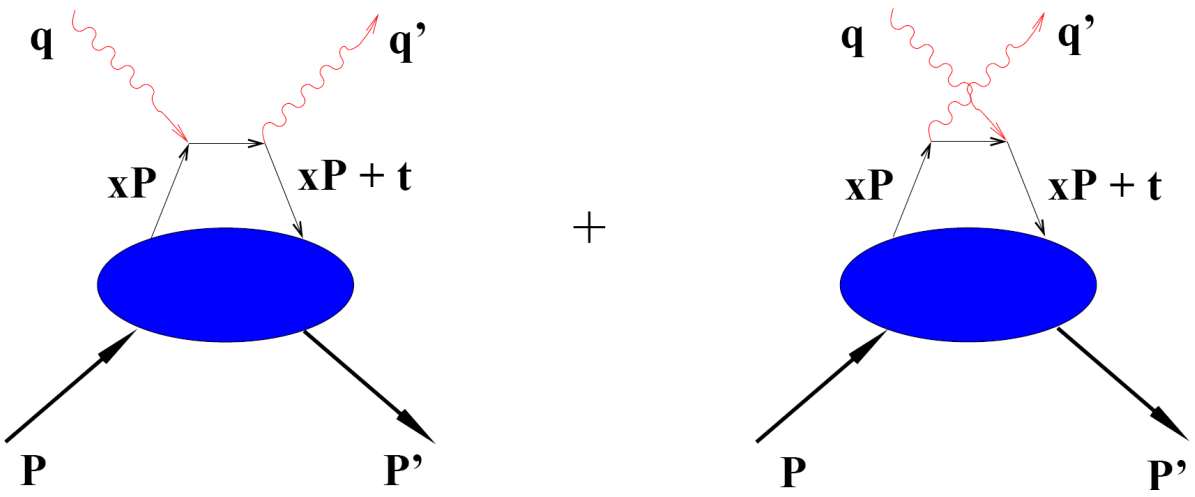


Figure 1: The handbag diagram for WACS.

structure functions, such as parton distribution functions (PDF) and form factors ($F_1$ and $F_2$). To NLO, only three of the four GPDs contribute to the WACS process: $H(x, \xi = 0, t)$, $\tilde{H}(x, \xi = 0, t)$, and $E(x, \xi = 0, t)$. Since the photons are both real, the skewness parameter $\xi$ is zero, reflecting the fact that the momentum absorbed by the struck quark is purely transverse. In the GPD approach to the handbag formalism, the WACS observables are new form factors of the proton that are $x^{-1}$-moments of the GPDs:

$$\begin{aligned} R_{_V}(t) &= \sum_a e_a^2 \int_{-1}^{1} \frac{dx}{x} H^a(x,0,t), \\ R_{_A}(t) &= \sum_a e_a^2 \int_{-1}^{1} \frac{dx}{x} \,\mathrm{sign}(x)\, \tilde{H}^a(x,0,t), \\ R_{_T}(t) &= \sum_a e_a^2 \int_{-1}^{1} \frac{dx}{x} E^a(x,0,t), \end{aligned} \tag{1}$$

where $e_a$ is the charge of the active quark and the three form factors are, respectively, the vector, axial vector, and tensor form factors ($\mathrm{sign}(x)$ is the sign of $\mathrm{x} \equiv \frac{x}{|x|}$). The corresponding form factors for elastic electron or neutrino scattering are given by the first ($x^0$) moments of the same GPDs:

$$
\begin{aligned}
F_1(t) &= \sum_a e_a \int_{-1}^{1} dx\, H^a(x,0,t), \\
G_A(t) &= \sum_a \int_{-1}^{1} dx\, \mathrm{sign}(x)\, \tilde{H}^a(x,0,t), \\
F_2(t) &= \sum_a e_a \int_{-1}^{1} dx\, E^a(x,0,t),
\end{aligned} \tag{2}
$$

where the three quantities are, respectively, the Dirac, axial, and Pauli form factors. On the other hand, the $t = 0$ limit of the GPDs produce the PDF's:

$$
\begin{aligned}
H^a(x,0,0) &= q^a(x), \\
\tilde{H}^a(x,0,0) &= \Delta q^a(x) \\
E^a(x,0,0) &= 2\frac{J^a(x)}{x} - q^a(x),
\end{aligned} \tag{3}
$$

where $J^a$ is the total angular momentum of a quark of flavor $a$ and is not directly measurable in DIS.

In the handbag factorization scheme in the symmetric frame, the WACS helicity amplitudes can be expressed as,

$$
\begin{aligned}
M_{\mu'+,\mu+}(s,t) &= 2\pi\alpha_{em}\left[\mathcal{H}_{\mu'+,\mu+}(s,t)(R_V(t)+R_A(t)) + \mathcal{H}_{\mu'-,\mu-}(s,t)(R_V(t)-R_A(t))\right], \\
M_{\mu'-,\mu+}(s,t) &= -\pi\alpha_{em}\frac{\sqrt{-t}}{m}\left[\mathcal{H}_{\mu'+,\mu+}(s,t) + \mathcal{H}_{\mu'-,\mu-}(s,t)\right] R_T(t),
\end{aligned} \tag{4}
$$

where $\mu(\nu), \mu'(\nu')$ denote the light-cone helicity of the incoming and outgoing photons (proton), respectively and $m$ is the mass of the proton. The signs on $M$ and $\mathcal{H}$ refer to the helicities of the proton and active quark, respectively. Each $\mathcal{H}$ represents the corresponding sub-process amplitude. This structure of the helicity amplitudes leads to a simple interpretation of the WACS form factors: $R_V \pm R_A$ is the response of the proton to the emission and reabsorption of quarks with helicity in the same/opposite direction of the proton helicity, and $R_T$ is directly related to the proton helicity-flip amplitude [32]. These equations lead to expressions relating WACS observables to the form factors.

The most important of these experimentally are the spin-averaged cross section, the recoil polarization observables and the initial-state helicity correlations $A_{LL}$ and $A_{LS}$. The spin-averaged cross section factorizes into a simple product of the Klein-Nishina (KN) cross section describing the hard scattering from a single quark, and a sum of form factors depending only on $t$ [31, 5]:

$$
\frac{d\sigma/dt}{d\sigma_{\mathrm{KN}}/dt} = f_V\left[R_V^2(t) + \frac{-t}{4m^2}R_T^2(t)\right] + (1-f_V)R_A^2(t)\,. \tag{5}
$$

For the interesting region of large $p_\perp$, the kinematic factor $f_{_V}$ is always close to 1. Consequently the unpolarized cross sections are largely insensitive to $R_{_A}$, and the left-hand-side of Eq. 5 is nearly $s$-independent at fixed $t$. One of the primary goals of E99-114 was to test this relationship as well as to determine the vector form factor $R_{_V}$. Calculations to NLO, which take into account both photon and proton helicity-flip amplitudes, do not change this prediction in any appreciable way [32, 37]. Updated cross section and Compton form factors (see Fig. 2) with their parametric uncertainties have also been evaluated [38].

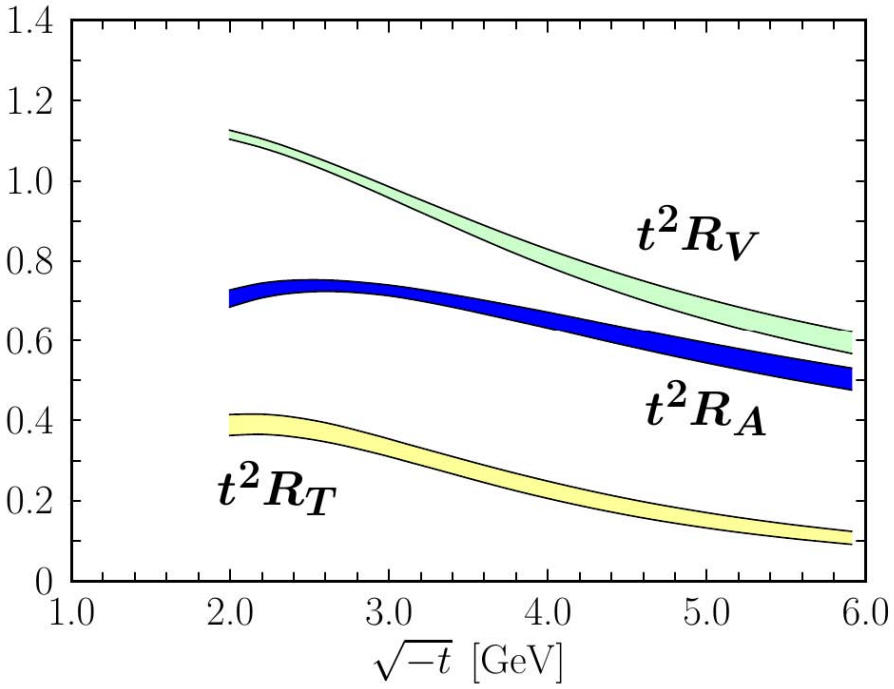


Figure 2: Predictions for the Compton form factors evaluated from the default fit in Ref. [32], scaled by $t^2$ and shown in units of GeV$^4$. The bands in each case show the parametric uncertainties.

The longitudinal and transverse polarization transfer observables, $K_{_{LL}}$ and $K_{_{LS}}$, respectively, are defined by

$$K_{_{LL}}\frac{d\sigma}{dt} \equiv \frac{1}{2}\left[\frac{d\sigma(\uparrow\uparrow)}{dt} - \frac{d\sigma((\downarrow\uparrow)}{dt}\right] \qquad K_{_{LS}}\frac{d\sigma}{dt} \equiv \frac{1}{2}\left[\frac{d\sigma(\uparrow\rightarrow)}{dt} - \frac{d\sigma(\downarrow\rightarrow)}{dt}\right] \tag{6}$$

where the first arrow refers to the incident photon helicity and the second to the recoil proton helicity ($\uparrow$) or transverse polarization ($\rightarrow$).

With definitions of two additional parameters,

$$\beta = \frac{2m}{\sqrt{s}}\frac{\sqrt{-t}}{\sqrt{s}+\sqrt{-u}} \qquad \kappa(t) = \frac{\sqrt{-t}}{2m}\frac{R_{_T}(t)}{R_{_V}(t)}\,, \tag{7}$$

the polarization observables are approximately related to the form factors by the expressions [5, 32],

$$K_{LL} \approx K_{LL}^{\rm KN} \frac{R_A(t)}{R_V(t)} \frac{1-\beta\kappa(t)}{1+\kappa^2(t)} \qquad \frac{K_{LS}}{K_{LL}} \approx \kappa(t) \frac{1+\beta\kappa^{-1}(t)}{1-\beta\kappa(t)} \tag{8}$$

where $K_{LL}^{\rm KN}$ is the longitudinal asymmetry for a structureless Dirac particle. These formulas do not include small gluonic corrections, which are discussed in Ref. [32].

The expressions above show that measurements of $K_{LL}$ and $K_{LS}$, when combined with measurements of $d\sigma/dt$, allow determinations of all three form factors. They also show that two very important pieces of information follow directly from the spin asymmetries: $K_{LL}$ and $K_{LS}$ / $K_{LL}$, which are directly related to the form factor ratios $R_A/R_V$ and $R_T/R_V$, respectively. For large energies and scattering angles near $\theta_p^{\rm cm}$= 90°, the $\beta$ terms are negligible small so the measurement is more direct [32].

The initial state helicity correlation observables are defined by,

$$A_{LL}\frac{d\sigma}{dt} \equiv \frac{1}{2}\left[\frac{d\sigma(\uparrow\uparrow)}{dt} - \frac{d\sigma((\downarrow\uparrow)}{dt}\right] \qquad A_{LS}\frac{d\sigma}{dt} \equiv \frac{1}{2}\left[\frac{d\sigma(\uparrow\rightarrow)}{dt} - \frac{d\sigma(\downarrow\rightarrow)}{dt}\right] \tag{9}$$

where the first arrow refers to the incident photon helicity and the second to the initial state proton helicity (↑). In the GPD approach of Ref. [32], the initial state observables are related to the final state observables:

$$A_{LL} = K_{LL} \qquad A_{LS} = -K_{LS}. \tag{10}$$

From the relationships connecting the WACS form factors to PDFs, the ratio $R_A/R_V$ is related to $\Delta q^a(x)/q^a(x)$. For WACS, the $e_a^2$-weighting of the quark flavors means that $u$ quarks will dominate the reaction. Moreover, at relatively large $-t$, the contributions to the form-factor integral are concentrated at moderate-to-high $x$, where the valence quarks dominate. Therefore, the $A_{LL}$ asymmetry contains direct information on $\Delta u(x)/u(x)$ in the valence region. Similarly, from the correspondence between WACS and electron scattering form factors, there is expected to be a close relationship between $R_T/R_V$ and $F_2/F_1$ [32]. The measurements of $G_E^p$ at JLab have shown that $F_2/F_1$ falls as $1/\sqrt{-t}$ rather than as $1/t$, the latter being predicted by pQCD [28, 29, 30]. It will be an important check on the theoretical interpretation of $F_2/F_1$ to see if $R_T/R_V$ behaves in a similar way. The results from E99-114 at $-t = 4$ GeV$^2$ are large but suggest that the $R_T/R_V$ may fall more rapidly with $-t$ than $F_2/F_1$. Experiment E07-002 has obtained better precision on $K_{LS}$ and $K_{LL}$, but its kinematic limitations make it difficult to say anything definite about the relationship between $F_2/F_1$ and $R_T/R_V$.

### Recent Developments

The experimental values of $K_{LL}$, although measured at relatively low values of $-t$ and $-u$, are large and positive, as shown in Fig. 3. This may be due to possible larger values of

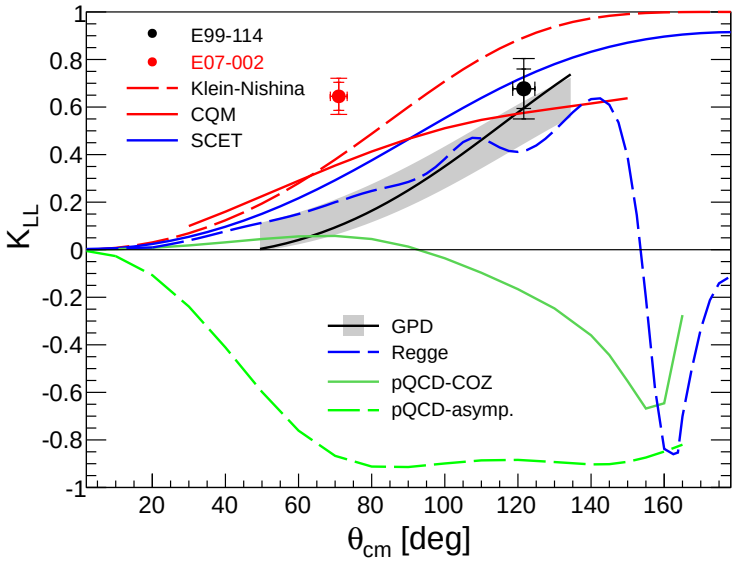


Figure 3: The recoil observable $K_{LL}$ measured in JLab experiments E99-114 and e70-002 as a function of scattering angle $\theta_{cm}$ [10].

$R_A$ than estimated in Ref. [38], suggesting that $R_A/R_V > 1$ and that there is actually an enhancement compared to the Klein-Nishina asymmetry. This was recently suggested by Kroll [11], who updated the predictions for $K_{LL}$ and $A_{LL}$ with a new profile function for the GPD $\tilde{H}$ fitted to data for the axial form factor $G_A$, which has been measured in neutrino scattering experiments to relatively poor precision and over a small range in $-t$. These updated predictions are shown for $A_{LL}$=$K_{LL}$ versus $\sqrt{-t}$ in Fig. 4 in the kinematic region where $-t$ and $-u$ are greater than 2.5 GeV$^2$. The black solid line in the figure corresponds to the new profile function, while the dashed line corresponds to the old one. The difference between them is evidence for how poorly constrained $\tilde{H}$ is in this kinematic regime. Likewise, Fig. 4 shows updated predictions for $A_{LS}$, which demonstrates how insensitive it is to target mass corrections.

The GPD handbag approach demonstrates that a measurement of both $A_{LL}$ and $A_{LS}$ at the same values of $s$ and $-t$ is an attractive option, as one can extract the Compton form factors $R_A$ and $R_T$ from the data with completely different observables not yet measured, while establishing the relationship between the other recoil observables. This would not only provide a crucial test of this handbag approach but also help in improving the parameterizations of the corresponding GPDs $\tilde{H}$ and $E$. The experimental measurements of $K_{LS}$ are in agreement within the experimental uncertainties with calculations for both the leading-quark and the pQCD approaches suggesting that there is no strong evidence for proton helicity flip in this reaction [39, 32, 12, 35, 40, 36]. The measurements seem to indicate that our understanding of $K_{LS}$ is correct over $\theta_p^{\rm cm}$. However the error bars are relatively large and

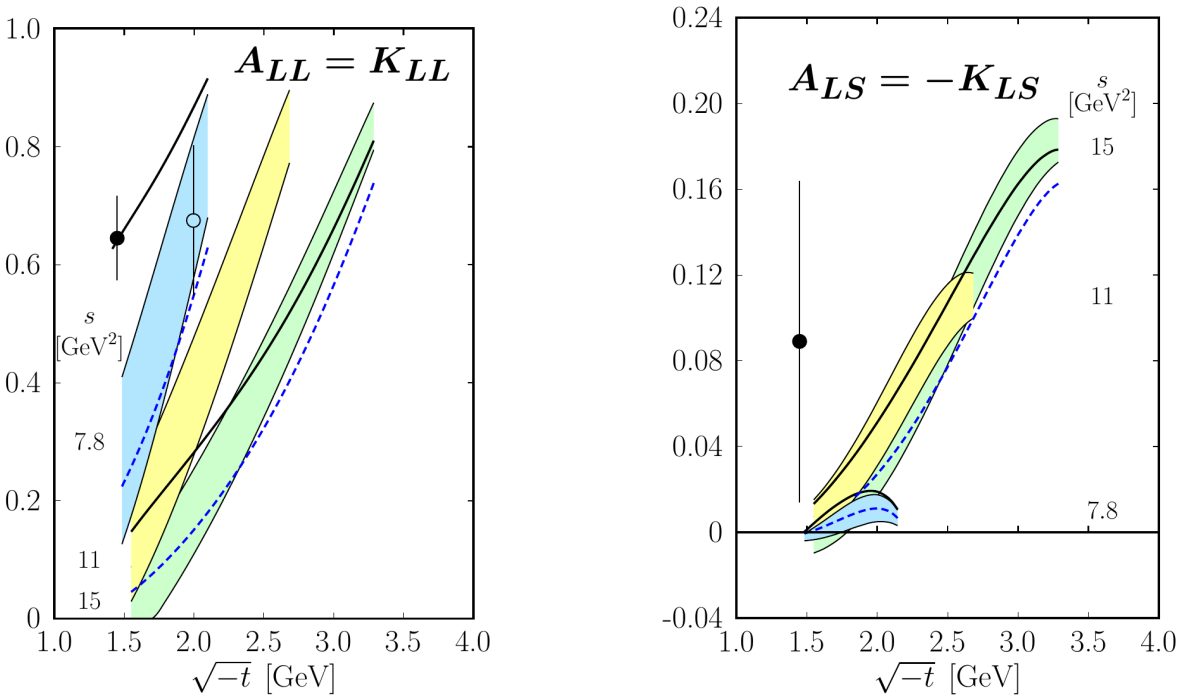


Figure 4: Predictions for the initial state helicity correlations $A_{LL}$ and $A_{LS}$ for the two scenarios discussed in Ref. [11] at $s$=7.8, 11, and 15 GeV$^2$. The highlighted areas show the extent of target mass corrections. The data points are $K_{LL}$ results from E99-114 (open circles) and E07-002 (closed circles).

new measurements of $A_{LS}$ will significantly improve the situation.

## 2.4 Soft-Collinear Effective Theory

There has been some criticism of the GPD-based approach, as it is a model which relies on parameterizing aspects of the assumed wavefunction. Therefore when computing the QCD radiative corrections there can be problems with the infrared behavior. Recently a complete factorization formula for the leading power contribution in wide-angle Compton scattering has been developed [35, 36]. In this approach, the Soft Collinear Effective Theory (SCET) is used to define the soft-spectator contribution in a field theoretical approach.

The SCET formalism follows the same handbag-based scheme as in the standard factorization approach, with the factorized formula for the WACS amplitudes written as the sum of two contributions to the scattering process. These amplitudes, denoted by $T_i$, can be described within the SCET approach by the factorization formula,

$$T_i(s,t) = T_i^{(h)}(s,t) + T_i^{(s)}(s,t), \tag{11}$$

where the hard spectator contribution $T^{(h)}$ is given by

$$T_i^{(h)}(s,t) = \mathbf{\Psi}(y_i) * H_i(s,t;x_i,y_i) * \mathbf{\Psi}(x_i) \tag{12}$$

expressing the convolution integrals with respect to the collinear fractions $x_i, y_i$. The soft spectator term is written as,

$$T_i^{(s)}(s,t) = C_i^q(s,t)\mathcal{F}_1 + C_i^g(s,t)\mathcal{G}_1, \tag{13}$$

where the coefficient functions $C_i^{q,g}$ describe a hard sub-process from quark and gluons, respectively, and the functions $\mathcal{F}_1$ and $\mathcal{G}_1$ describe the hard-collinear and soft interactions and represent new SCET form factors (Fig. 5).

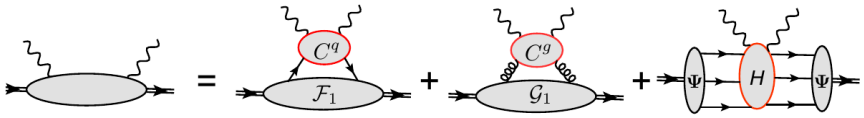


Figure 5: The diagrams for WACS factorization with the soft-overlap contributions described by the SCET FFs $\mathcal{F}_1$ and $\mathcal{G}_1$ from Ref. [35].

One advantage of the SCET formalism is that it represents a systematic approach to the factorization of the hard and soft sub-processes, leading to clearly defined predictions that are not sensitive to parameterization for the region where $|t|$ and $|u|$ are greater than 2.5 GeV$^2$. The WACS observable $K_{LL}$ has been studied to leading-order and next-to-leading order approximations which include both kinematic power corrections and nucleon helicity flip contributions. A comparison for this observable against JLab data as a function of the scattering angle $\theta_{cm}$ can be seen in Fig. 6. The relationship between $K_{LL}$ and $A_{LL}$ has been studied, the results of which indicate that $K_{LL}(\theta_{cm}) \simeq A_{LL}(\theta_{cm})$ to all orders in $\alpha_s$ at leading power and with near negligible $s$-dependence [36, 41].

The SCET approach predicts that $K_{LL} = K_{LL}^{KN}$ at leading-order, where $K_{LL}^{KN}$ is the Klein-Nishina asymmetry, with NLO corrections causing a small reduction in the predicted values. The number of parameters in the SCET approach is considerably smaller than in the GPD model and there is a strict *weak* $s$-dependence. Therefore large deviations in $A_{LL}$ at fixed $\theta_{cm}$ and different values of $s$ would imply a break-down of factorization. In the SCET framework it also predicted that $K_{LS} = -A_{LS}$, although the predicted values for this observable exhibit different behavior from that of the GPD model. This is clear from Fig. 7, which shows the SCET prediction [41] for the same three $s$ values as shown for the GPD model in Fig. 4.

## 2.5 The Relativistic Constituent Quark Model

The relativistic constituent quark (RCQ) model was developed by Miller [12] and has been successful in describing the electromagnetic nucleon form factors [42] and WACS data [8, 7].

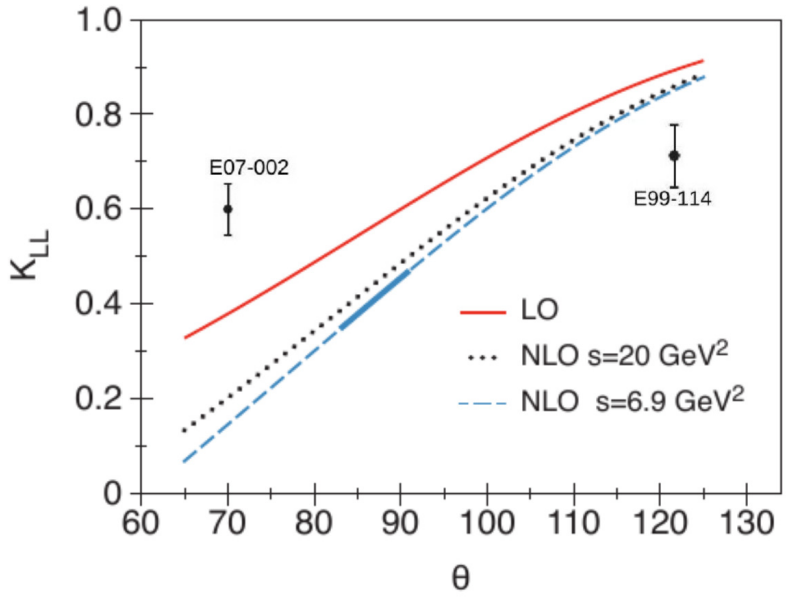


Figure 6: The longitudinal asymmetry $K_{LL}$ as a function of scattering angle $\theta$. A comparison of the LO (red) and NLO calculated with $s = 6.9$ GeV$^2$ (dashed) and $s = 20$ GeV$^2$ (dotted) lines [36].

In this approach Poincare invariance, gauge invariance, conservation of parity, and time reversal invariance are respected in an impulse approximation evaluation of the handbag diagram. The model attempts to evaluate the handbag in a way that avoids neglecting the effects of hadronic helicity non-conservation, such that relativistic and quark mass effects induce significant quark transverse and orbital angular momentum.

The model starts with a wave function for three relativistic constituent quarks:

$$\Psi(p_i) = u(p_1)u(p_2)u(p_3)\psi(p_1, p_2, p_3),$$

where $p_i$ represents space, spin, and isospin indices. The wave function is evaluated in light cone variables and includes quark mass effects and proton helicity flip. Due to lower components of Dirac spinors, where the quark spin is opposite to that of the proton, quark orbital angular momentum appears.

The polarized observables involve helicity amplitudes determined by making a unitary transformation on the spin amplitudes $\mathcal{M}_{S',S}(\boldsymbol{\epsilon}', \boldsymbol{\epsilon})$:

$$\Phi_{\mu'\lambda',\mu\lambda} = \sum_{S',S} T^*(\mathbf{p}')_{S'\lambda'} \mathcal{M}_{S',S}(\boldsymbol{\epsilon}'_\mu, \boldsymbol{\epsilon}_\mu) T_{S,\lambda}(\mathbf{p}) \tag{14}$$

where $\mu$, $\lambda$ represent the helicity of the initial photon and initial proton, and $T_{S,\lambda} \equiv \bar{u}(p,s)u_H(p,\lambda)/2M_p$ in which $u$ represents an ordinary Dirac spinor and $u_H$ represents a helicity spinor.

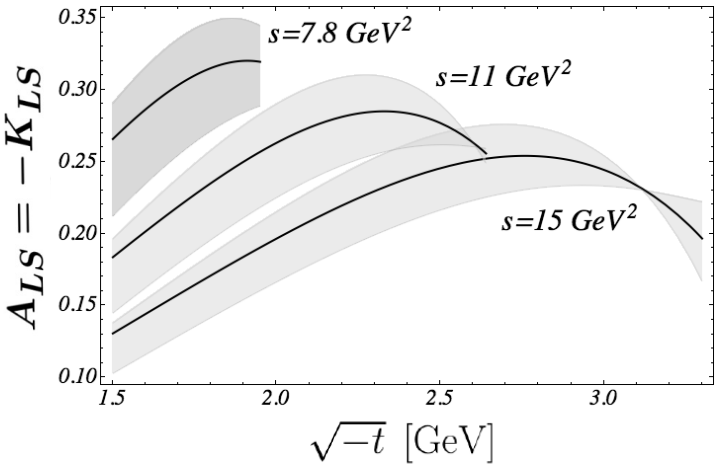


Figure 7: The prediction for $A_{LS} = -K_{LS}$ for SCET for $s = 7.8$, 11 and 15 Gev$^2$ over a range of $\sqrt{-t}$ with theoretical uncertainty represented by the gray band [41].

The differential cross section and the spin-dependent observables are then expressed in terms of these amplitudes. The relationship between differential cross section and $K_{LL}$ and $A_{LL}$ has a similar form to the GPD approach, except that the dependence of $\mathcal{M}_{S',S}$ on the photon polarization vector is suppressed. Equality of $\Phi_2$ and $\Phi_6$ in the GPD approach can only occur if each of the proton spin flip matrix elements vanish, or if their sum vanishes. In this model, however, inspection of the Compton quark scattering operator shows that the spin-flip matrix elements do not vanish and $\Phi_2 \neq \Phi_6$. As a result $A_{LL}$ and $K_{LL}$ deviate for larger center-of-mass angles. The resulting predictions for the polarization observables $A_{LL}$ and $K_{LL}$ are shown in Fig. 8, together with data from the E99-114 and E07-002 experiment. The most striking consequence of Miller's results is an increasing deviation between $A_{LL}$ and $K_{LL}$ at larger scattering angles, which can be tested experimentally. The same is true for the prediction that the transverse polarization observable $K_{LS} = A_{LS} = 0$.

## 2.6 Summary of Physics Goals

It is important to realize that the issues raised at the start of this section are not limited to the WACS reaction. Indeed, they are questions that need to be addressed for all studies of the nucleon using exclusive reactions in the hard scattering regime. The old paradigm for addressing them was the pQCD mechanism and the distribution amplitudes. It is quite likely that the new paradigm will be the handbag mechanism and GPDs. In any case, the applicability of factorization itself needs to be tested, not only over a wide range of kinematic variables but also over a wide range of observables and different reactions. Of

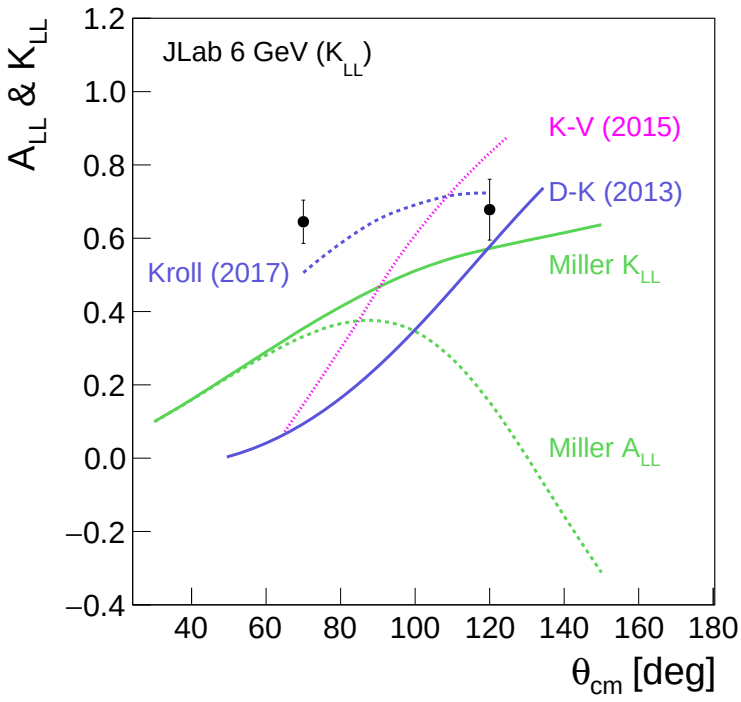


Figure 8: Predictions for $A_{LL}$ in the GPD approach of Diehl and Kroll [38], the SCET approach of Kivel [36] and CQM model of Miller [12] and data on $K_{LL}$ from E99-114 and E07-002. Kroll's recent update based on a new profile function of $\tilde{H}$ is also shown [11].

these, the WACS polarization observables $A_{LL}$ and $A_{LS}$ are unique in their sensitivity to the proton's axial and tensor structure at high momentum transfer.

The priority for the current proposal is the measurement of both $A_{LL}$ and $A_{LS}$ over a broad range of $s$ and $-t$ in the kinematic regime where factorization should be unambiguously applicable. Taken with the differential cross section data which will be obtained in E12-14-003, this will allow for the extraction of $R_A/R_V$ and $R_T/R_V$ in the GPD approach. This will not only help to establish the relationship between $F_2/F_1$ and $R_T/R_V$, but crucially provide systematic improvements to the parameterizations of the underlying GPDs, $\tilde{H}$ and $E$. Given that the SCET form factor $\mathcal{R}$ has been calculated directly from E99-114 cross section data, the proposed polarized measurements will not only help determine the validity of this factorization approach, but will significantly reduce the theoretical ambiguity by providing the needed constraints on the power corrections and non-perturbative matrix elements.

We therefore propose measurements in of $A_{LL}$ at $\theta_p^{\rm cm}$=70°, 90° and 110° and $A_{LS}$ at $\theta_p^{\rm cm}$=70° and 110°. These measurements will cover a range in $s$ of 9 to 20 GeV$^2$, and a range in $-t$ of 2.8 to 8.1 GeV$^2$. With such data it will be possible to:

1. Make an explicit, model-independent test of factorization by measuring the $s$-dependence

of the polarization observables at fixed $\theta_p^{\rm cm}$, and verify that target mass corrections and higher twist effects are small.

2. Systematically improve our knowledge of the non-perturbative matrix elements of the handbag mechanism in the GPD and SCET approaches. This is particularly important for the GPDs $\tilde{H}$ and $E$ at high $-t$, which can be accurately measured from the form factor ratios $R_{_A}/R_{_V}$ and $R_{_T}/R_{_V}$. This will have a significant and broad impact in the fields of electron and neutrino scattering.

3. By comparing model predictions for both polarization observables, test how the WACS reaction proceeds, either via the interaction of photons with a current quark or with a constituent quark. This will also allow for an unambiguous determination of which of the three leading handbag approaches best describes the data.

# 3 Experimental Setup

The proposed experiment will study the scattering of polarized photons from a polarized ammonia target, as illustrated in Fig. 9. The scattered photon will be detected by the Neutral Particle Spectrometer (NPS), while BigBite arranged as a proton spectrometer will be used to detect the recoiling proton. The photon source includes a 10% radiator located 2 m upstream of the target, producing a narrow (0.9 mm diameter on target) untagged photon beam. Incident electron beam energies of 8.8 and 11 GeV will be used at a beam current of 2.5 $\mu A$ and 80% polarization. Such currents are large enough to enable precision beam measurements ensuring stable, high-quality primary beam delivery. The target will be a polarized ammonia device, the so called UVA/JLAB polarized target, operating in a 5 Tesla field pointing along the beam line (longitudinal) or perpendicular to it (transverse). One advantage of such a large target field is that low-energy charged particles will be deflected away from the detector systems.

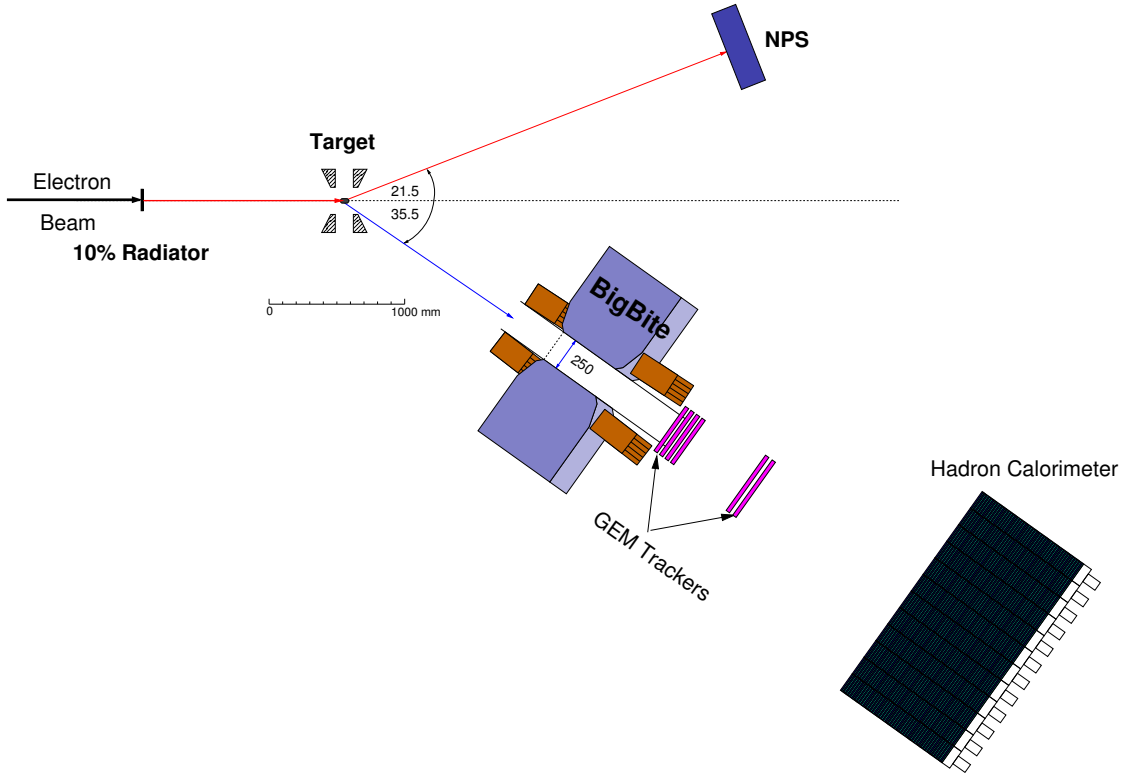


Figure 9: Schematic of the experimental setup, with the scattered photon detected by the NPS and the recoil proton detected by BigBite (kinematic setting L1).

With an electron beam of 100 nA intensity on the UVA/JLAB polarized target, an average $NH_3$ polarization of 75% has been achieved in several experiments (RSS and SANE

experiments in Hall C, and $g_2^P$ and $G_E^P$ in Hall A). A pure photon beam on target allows for simpler operation and higher average polarization. The beam polarization will be measured to an accuracy of 1% with the Hall C Möller polarimeter. Continuous online monitoring of the beam polarization will be possible due to the large cross section and helicity asymmetry for $\pi^0$ photoproduction, as determined in E99-114.

## 3.1 The Polarized $NH_3$ Target

This experiment will use the UVA/JLAB polarized target, which has been successfully utilized in E143/E155/E155x experiments at SLAC and E93-026, E01-006, E07-003, E08-007 and E08-027 at JLab. E08-007 and E08-027 used a different superconducting split Helmholtz pair, originally part of the Hall B polarized target. The coil package is very similar to the original one. See Fig. 10 for a cross-sectional view of the target. The target polarization will be oriented both longitudinal and transverse (within 5°) to the beam, made necessary for acceptance issues.

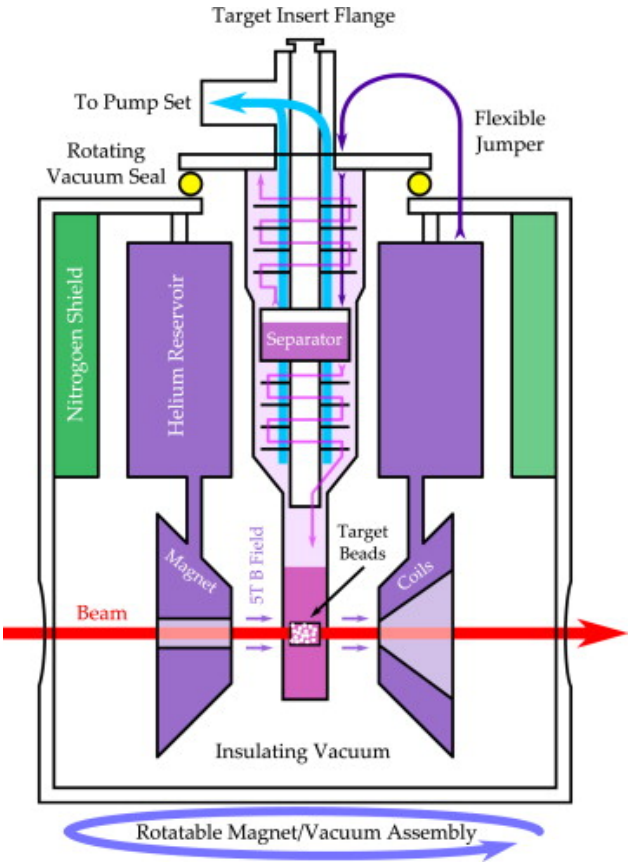


Figure 10: Cross-sectional view of the polarized target (taken from Ref. [43]).

This target operates on the principle of Dynamic Nuclear Polarization (DNP). The low

temperature (1 K), high magnetic field (5 T) natural polarization of solid materials (ammonia, lithium hydride) is enhanced by microwave pumping. The polarized target assembly contains two 3–cm–long target cells that can be selected individually by remote control to be located in the uniform field region of the magnet. There are also two other target cells which are available for a calibration target (carbon foil or $CH_2$). The permeable target cells are immersed in a vessel filled with liquid helium and maintained at 1 K by using a high power evaporation refrigerator. The magnet coils have a 55° conical shaped aperture along the axis and a 38° wedge shaped aperture along the vertically oriented mid-plane.

The target material is exposed to 140 GHz microwaves to drive the hyperfine transition which aligns the nucleon spins. The DNP technique produces proton polarizations of up to 95% in the $NH_3$ target. The inexorable fall in polarization due to radiation damage in an electron beam will be markedly reduced with a pure photon beam and we will be able to avoid much of the overhead spent in annealing the radiation damage away. It is estimated that the time spent on this exercise to recover from the radiation damage will be reduced by two-thirds. As part of the program to minimize the sources of systematic errors, the target polarization direction will be reversed after each anneal by adjusting the microwave frequency.

Experience has shown that a 100 nA beam of electrons imposes a heat load of approximately 0.3 W on the target system. Microwaves contribute up to a further 1 W and the two sources exhaust the cooling power of the $^4$He refrigerator. Geant4 simulations have been preformed in order to assess the impact of moving to a pure photon beam. It was found the power deposited in the target cup by a photon beam produced by an 8.8 GeV, 1 $\mu A$ electron beam was 0.117 W for a 10% radiator, which suggests that the heat load associated with a 2.5 $\mu$A beam on the radiator will not reach the cooling power limit of the target refrigerator.

**Uniform illumination of the target cups**

Solid polarized targets suffer from radiation damage and local hot spots can also cause depolarization of the target while the embedded NMR coil samples the polarization over the entire cup. In order to minimize the production of these hot spots and to ensure accurate NMR readings electron beams have been rastered over the target cup face. This slow raster spirals over the approximate 1 in$^2$ area of the target face, and when combined with the standard fast raster (2 mm square) ensures that the target receives a uniform dose. This is not possible with the photon beam, but could be achieved with HCPS by creating several horizontal slots in the central insert and slow movement of the electron beam along those slots. The uniform illumination of area of the target between slots require vertical motion of the central insert as was designed Ref. [19]. However, uniform exposure of the target cell can still be achieved by a combined rotation of the target cup synchronized with an up/down movement of the target ladder, as shown in Fig. 11. Rotation of the beam cup is already part of the UVa target group's practice, albeit for different reasons than presented here. More details on this style of raster can be found in the HIPS workshop proceedings [22].

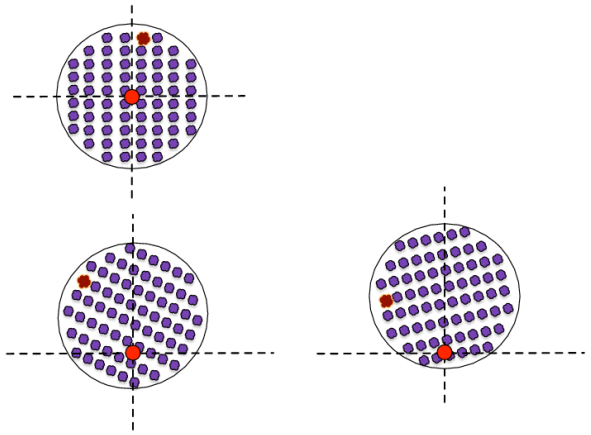

Figure 11: Vertical motion combined with rotation of cup will allow uniform coverage of target cell. The red dot represents the fixed position of the photon beam. The colored bead in the cup can be seen moving as the cup rotates counterclockwise and the target ladder is moved up. Over time the target receives a full and uniform exposure [22].

## 3.2 The Neutral Particle Spectrometer

There is a substantial overlap between key participants in the current proposal and the Neutral Particle Spectrometer (NPS) collaboration, who will build the NPS (see Ref. [44] for details) for this and other proposed and approved experiments – for example, the WACS differential cross section experiment (E12-14-003). It is a $PbWO_4$ calorimeter, the sensitive region of which is 30 (horizontal) x 36 (vertical) inches, sitting on a frame allowing for easy movement, as shown in Fig. 12. The position resolution of the NPS is 3 mm and the energy resolution, $\sigma_E/\sqrt{E}$, is better than 3%. For the proposed experiment the NPS will be placed at a range of angles from 17.4° to 42.3° and a range of distances from the pivot from 1 m to 3 m. Comparing directly with calculations for similar kinematic settings in E12-14-003, which uses a high current mixed electron-photon beam and simply scaling by luminosity, the maximum singles rate per crystal is expected to be less than 50 kHz. Likewise, the accumulated dose is expected to be less than 10 krad. Both are well within the capabilities of the calorimeter.

## 3.3 The BigBite Spectrometer

The BigBite spectrometer is a large acceptance non-focusing magnetic spectrometer, which has been used in several 6 GeV era experiments and is intended for use as an electron spectrometer in 12 GeV experiments such as E12-09-018 [45] and E12-09-019 [46] (as shown in Fig. 13). For 12 GeV running, in order to enable detection of high momentum particles, the MWDC trackers are to be replaced by GEM detector planes developed as part of the Super BigBite Spectrometer (SBS) project [47]. The GEM detectors have been designed in

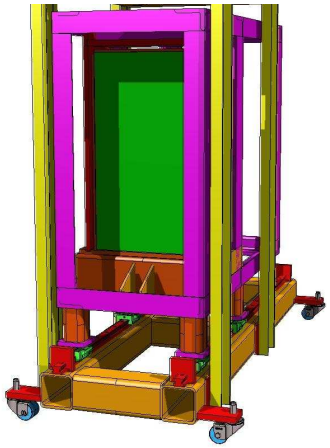

Figure 12: The front view of the Neutral Particle Spectrometer (NPS) [44].

a modular form specifically to allow them to be configured for use with BigBite as well as the SBS. The momentum resolution in this configuration is anticipated to be $\sigma_p/p = 0.5\%$ with angular resolution better than 1 mrad in both dispersive and non-dispersive directions. BigBite will cover a range of angles between 19.4° and 35.5°, with a distance between pivot and dipole entrance of 3.5 m for the smaller angle settings and 1.5 m at larger angles. The expected rate in the GEM trackers is around 1 kHz/cm, which is well within the capability of these detectors. Charged pion rates are at worst around half of the proton rate, meaning that dedicated particle identification detectors are not needed. Therefore, in addition to the GEM planes, the only other detector needed for timing and triggering is the SBS hadron calorimeter (HCAL). If installation of HCAL proves difficult, the scintillators used in the BigHand system could also be used as a trigger detector provided they provide sufficient rate capability.

## 3.4 The Photon Source

The experimental program laid out in this proposal requires a real photon source. At JLab, Halls B and D have built-in real photon capabilities, but those sources are designed for a tagged photon beam with an intensity of $10^7$ Hz, which is many orders of magnitude below the intensity required for a WACS experiment at 8-10 GeV. One of the primary tasks of the WACS collaboration is to propose an optimum concept, design, simulate and build a high intensity photon source that can provide required intensity with sufficiently low radiation in the hall, especially in the target and detector area during operation and soon after beam shutdown. After a decade of considering the technical challenges, a conceptual solution was found and presented at the NPS collaboration meeting in November 2014 [48, 19].

This solution is based on the observation that with one meter of heavy shielding a hermetic source could be constructed because the opening channel for the incident electron

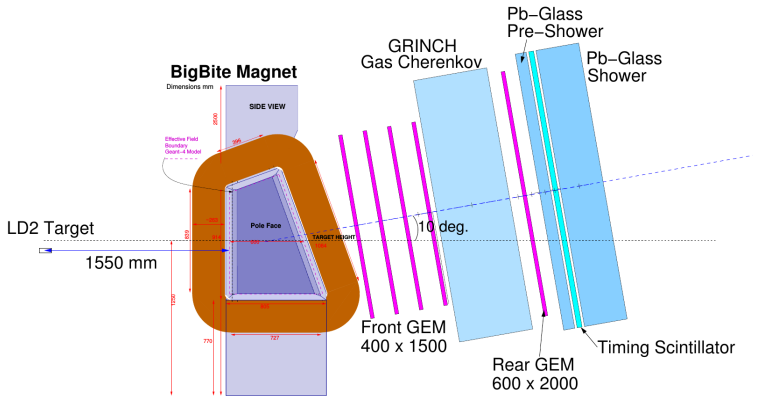


Figure 13: The 12 GeV BigBite detector configuration (set up as an electron spectrometer in this particular case). For running as a proton spectrometer in Hall C, the GRINCH, timing scintillators and shower counters will be replaced with HCAL or BigHand scintillators.

beam and produced photon beam needs to be just 2 mm in diameter for such a compact size of the source (overall 3x3x3 $m^3$). The radiation will be produced inside and contained (except of course the photon beam) because the source is hermetic (HCPS). The concept also provides a small photon beam spot at the target which is very important for data analysis and background suppression. The magnetic deflection of the beam is an obvious way to cleanly separate the photon and electron beams. However, the challenge of beam power absorption required a new solution. The standard dump for 1 MW beam power has a reliable but complicated design. However, even for our case of 30 kW beam power, local peaks in power density could melt the absorber. We noticed that for the proposed 2.5 T field for the cleaning magnet and a 2 mm vertical size of the opening channel in the magnet leads to the desirable small incident angle of electron entry to the absorber. When combined with a 1 mm vertical raster of the beam, the area of power deposition become 30 cm long and local power density is well within operational regime for proposed WCu absorber.

The technical parameters of the source components are modest in complexity:

- a 10 % radiator;
- a compact 1 m long magnet with 2.5 T field in small 3 cm wide gap (designed);
- an inner absorber of WCu alloy;
- low cost W-powder for outer shielding.

More detailed information on the photon source, prompt radiation levels, activation and beam power capabilities can be found in Ref. [22]. For the purposes of the current proposal, it is simply assumed that the beam parameters are defined by a 2 m radiator-to-target distance

and 2.5 $\mu A$ primary electron beam current, corresponding to an integrated photon flux on target ($> 0.5 E_{\mathrm{Beam}}$) of $1.5 \times 10^{12}$ s$^{-1}$.

# 4 Proposed Measurements

An 80% longitudinally polarized electron beam with a current of 2.5 $\mu$A at energies of 8.8 GeV and 11 GeV will be used in the proposed experiment. A 10% radiator, together with high intensity photon source will produce a narrow, untagged bremsstrahlung photon beam. This photon beam will strike a 3 cm-long $NH_3$ longitudinally and transversely polarized target. The BigBite spectrometer will detect the recoil proton, while the scattered photon will be detected by the Neutral Particle Spectrometer (NPS). The angle and distance from the target for each spectrometer were optimized via Geant4 simulation. The following subsections give details on the proposed kinematic settings, the most significant background processes, the expected count rates for WACS events, and finally a discussion of systematic uncertainties.

## 4.1 Kinematic Settings

Table 1 shows the range of kinematic settings that were considered for the current proposal. In order to maximize the physics impact while simultaneously keeping the beam-time request as low as achievable, some of the settings were rejected. This was done either as a result of poor projected statistical precision, low physics impact or, for one setting, the polarized target coils directly affecting the detector acceptance.

| $\theta_p^{\rm cm}$ | $E_{\rm Beam}$ | $A_{LL}$ | $A_{LS}$ |
|---|---|---|---|
| 70° | 8.8 GeV | ✓ | ✓ |
| 70° | 11.0 GeV | ✓ | × (low physics impact) |
| 90° | 8.8 GeV | ✓ | × (acceptance outside target opening) |
| 90° | 11.0 GeV | × (low count rate) | × (low count rate) |
| 110° | 8.8 GeV | ✓ | ✓ |
| 110° | 11.0 GeV | × (low count rate) | × (low count rate) |

Table 1: Kinematics setting considered for the current proposal.

The final set of proposed measurements therefore include four kinematic settings with the target polarization oriented in the longitudinal direction (L1-4) and two settings with it oriented in the transverse direction (S1 and S4). Five of the settings will take data with an 8.8 GeV electron beam, while the L2 setting relies on using an 11 GeV beam. These six kinematic points are summarized in Table 2. The two-body kinematic correlation between the recoil and scattered particles means that a central value and range of incident photon energy is uniquely defined by the detectors' angle and acceptance. The kinematic variables in the table correspond to this central setting, which is significantly below the bremsstrahlung endpoint in order to facilitate the $s$-scans.

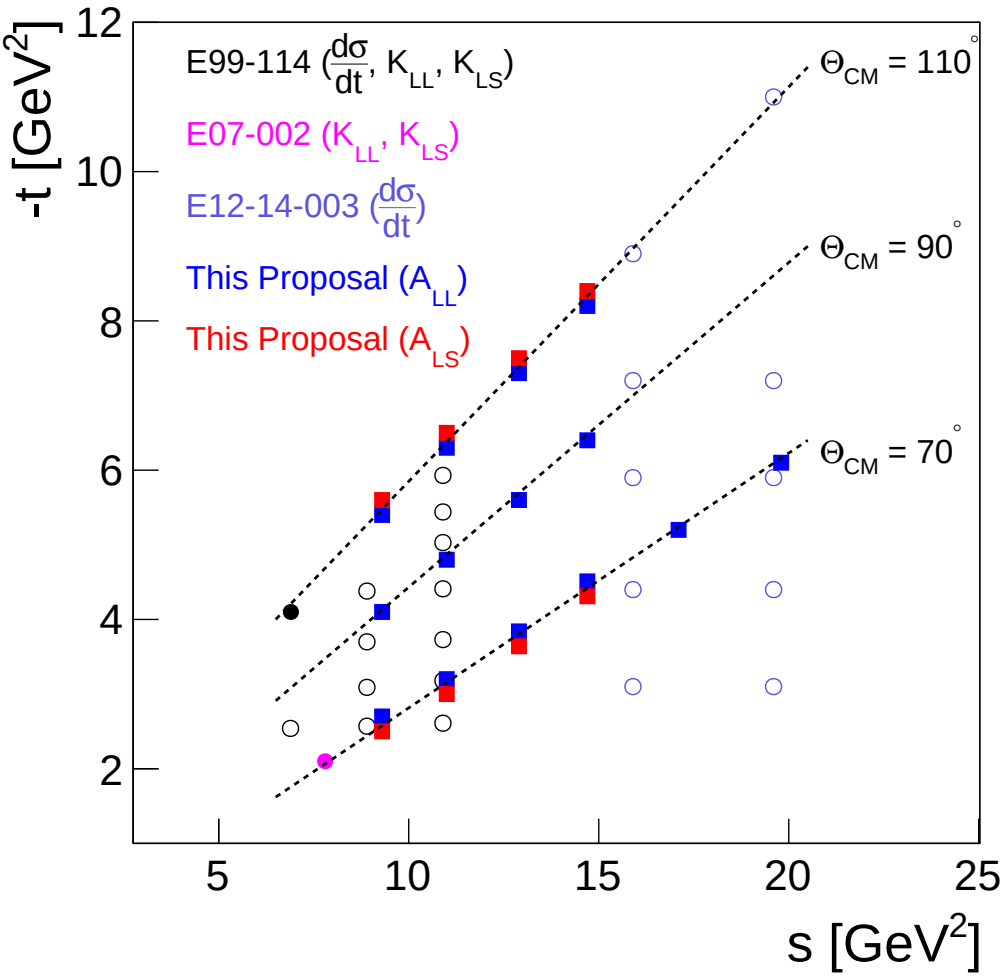


Figure 14: The kinematic coverage (Mandelstam variable $t$ as a function of $s$) of the current proposal taking into account the BigBite and NPS acceptances (square symbols). The diagonal lines correspond to 70, 90, and 110° CM angles. Data points from previous and planned JLab experiments (circle symbols) are also shown.

| Kin | $E_{\text{Beam}}$ [GeV] | $P_{\text{Target}}$ | $E_{\text{in}}$ [GeV] | $\theta_\gamma$ [°] | $E_\gamma$ [GeV] | $D_{\text{NPS}}$ [m] | $\theta_{\text{p}}$ [°] | $p_{\text{p}}$ [GeV/$c$] | $D_{BB}$ [m] | $\theta^{\text{cm}}$ [°] |
|---|---|---|---|---|---|---|---|---|---|---|
| L1 | 8.8 | L | 6.0 | 21.5 | 4.16 | 3.0 | 35.5 | 2.62 | 1.5 | 70.0 |
| S1 | 8.8 | T | 6.0 | 21.5 | 4.16 | 3.0 | 35.5 | 2.62 | 1.5 | 70.0 |
| L2 | 11.0 | L | 9.5 | 17.4 | 6.49 | 3.0 | 30.5 | 3.82 | 1.5 | 70.0 |
| L3 | 8.8 | L | 6.0 | 30.2 | 3.22 | 3.0 | 26.5 | 3.63 | 2.5 | 90.0 |
| L4 | 8.8 | L | 6.0 | 42.3 | 2.25 | 1.0 | 19.4 | 4.55 | 3.5 | 110.0 |
| S4 | 8.8 | T | 6.0 | 42.3 | 2.25 | 1.0 | 19.4 | 4.55 | 3.5 | 110.0 |

Table 2: Kinematics variables for WACS in four settings with a longitudinally polarized target (L1–L4) and two settings with a transversely polarized target (S1 and S4).

The large acceptance of both the BigBite and NPS detector systems allows the data to be divided into several bins in $s$ per kinematic setting. There is some flexibility in how this binning is done, but for the purposes of count rate estimates, the 8.8 GeV points are binned according to a reconstructed incident energy range of 4-5 GeV, 5-6 GeV, 6-7 GeV and 7-8 GeV. For the 11 GeV setting (L2) as a result of lower counting rates, the data is divided into two wider bins in incident energy (8-9.5 GeV and 9.5-11 GeV). This means there are 22 data points (14 for $A_{LL}$ and 8 for $A_{LS}$) for the six kinematic settings that were chosen. This is best seen in Fig. 14, which shows the kinematic coverage for the current proposal. As can be seen from the circles on the figure, the kinematics are well-matched to those proposed for E12-14-003.

## 4.2 Physics Backgrounds

Previous JLab experiments have shown that utilization of the two-body kinematic correlation between recoil proton and scattered photon (co-planarity) results in clean extraction of WACS events over two main background processes: events corresponding to the detection of one photon from the decay of a photo-produced neutral pion, and elastic electron-proton scattering events. This radiative part of this latter background contribution is difficult to separate from the WACS events and leads to a substantial contribution to the overall systematic uncertainty. One significant advantage of the deployment of a pure photon source is that this background will not be present in the proposed set of measurements.

The primary background therefore comes from neutral pion photo production from the protons in the target. It can be separated only on a statistical level using the difference in the shapes of the distribution of WACS and H($\gamma, \pi^0$) events. This background leads to a large dilution factor, which affects the statistical accuracy of the measurements. The pion can also be produced from bound protons in nitrogen. Motion of the nucleons in nuclei, and FSI, reduce dramatically the dilution of WACS events. The nuclear pion process was investigated by using E99-114 data obtained with an aluminum target, and it was found

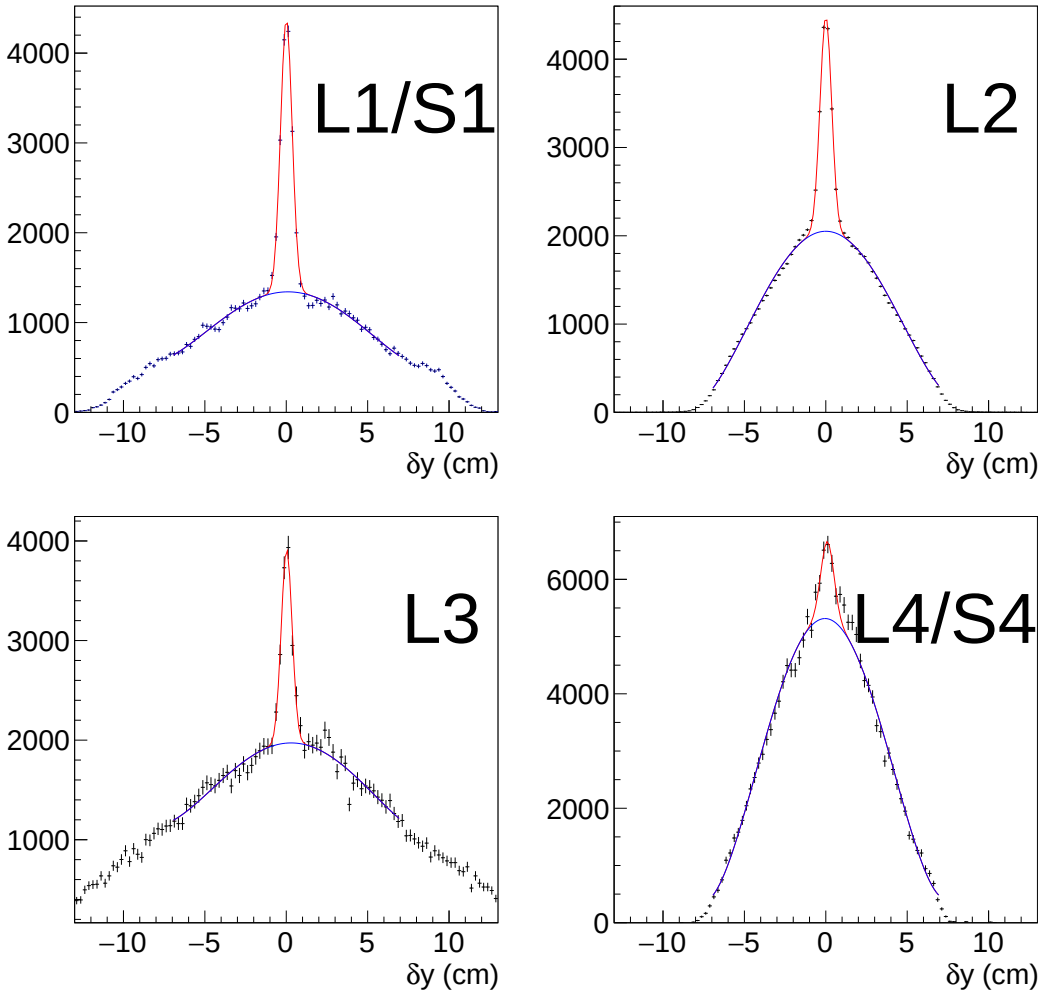


Figure 15: Subtraction of background events for one bin in each kinematic setting (note that the distributions of L1 and S1, and L4 and S4, will be very similar). The fit to WACS events is shown in red, while the background fit is shown in blue.

that at conditions similar to those proposed here, pions produced from nuclei increase the dilution factor by less than 10%.

The dilution factor $D$ quantifies the ratio between the total number of events recorded in the central co-planar region and the actual number of WACS events. It has been calculated for each of the proposed $s$ bins using a Geant4 simulation of the experimental setup, with cross sections extrapolated from E99-114 data. Typical kinematic co-planar distributions are shown in Figure 15 for one $s$ bin in each kinematic setting. The dilution factor was found to vary between $D = 1.6$ for kinematic point L1 and $D = 6.2$ for kinematic point L4.

## 4.3 Production Event Rate

The event rate is the product of the luminosity, the cross section, and the acceptance of the detectors, as well all other factors such as DAQ dead time and detection efficiency. The rate $N_{\text{WACS}}$ can be calculated as:

$$N_{\text{WACS}} = \frac{d\sigma}{dt}\frac{(E_\gamma^f)^2}{\pi}\Delta\Omega_\gamma f_{\gamma p} N_p N_\gamma \,,$$

where $\frac{d\sigma}{dt}$ is the WACS cross section, the factor $\frac{(E_\gamma^f)^2}{\pi}$ is the Jacobian that converts $dt$ to $dEd\Omega$, $\Delta\Omega_\gamma$ is the solid angle of the WACS events, $f_{\gamma p}$ is the BigBite-NPS acceptance, $N_\gamma$ is the number of incident photons per unit time, and $N_p$ is the number of target protons per unit area.

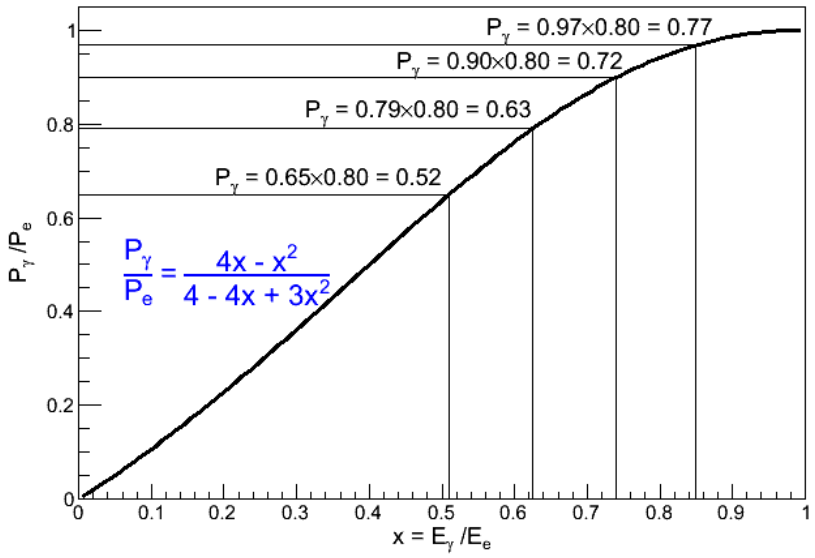


Figure 16: Ratio of the photon and electron polarization as a function of their energies.

A Geant4 simulation has been used to calculate this rate for each of the 22 data points. It was found that for the central $s$ bins, the WACS cross section varies between $6.4 \times 10^{-36}$ cm$^2$/GeV$^2$ (L4) and $410 \times 10^{-36}$ cm$^2$/GeV$^2$ (L1), while the $f_{\gamma p}$ acceptance factor varies between 0.1 (L4) and 0.4 (L2). The number of proton nuclei in the target was computed using the formula:

$$N_p = \frac{Z}{A} t f_{pack} N_A \,.$$

For the UVA/JLAB target the estimate is $N_p = 1.65 \times 10^{23}$ protons/cm$^2$. Assuming a 2.5 $\mu$A beam intensity and a 10% copper radiator, the expected photon flux between 4 and 8 GeV for an 8.8 GeV electron beam is $1.5 \times 10^{12}$ s$^{-1}$, and $6.2 \times 10^{11}$ s$^{-1}$ between 8 GeV and the endpoint for an 11 GeV electron beam.

| Kin | $E_{\text{in}}$ Range [GeV] | $N_{\text{WACS}}$ [$h^{-1}$] | $D$ | $\Delta A_{LL}$ | $\Delta A_{LS}$ | Time [h] |
|---|---|---|---|---|---|---|
| L1 | 4 – 5 | 550 | 1.6 | 0.02 | - | |
| L1 | 5 – 6 | 550 | 1.7 | 0.02 | - | |
| L1 | 6 – 7 | 228 | 1.8 | 0.03 | - | |
| L1 | 7 – 8 | 53 | 1.9 | 0.05 | - | 50 |
| S1 | 4 – 5 | 550 | 1.6 | - | 0.02 | |
| S1 | 5 – 6 | 550 | 1.7 | - | 0.02 | |
| S1 | 6 – 7 | 228 | 1.8 | - | 0.03 | |
| S1 | 7 – 8 | 53 | 1.9 | - | 0.05 | 50 |
| L2 | 8 – 9.5 | 52 | 2.4 | 0.05 | - | |
| L2 | 9.5 – 11 | 23 | 2.5 | 0.08 | - | 50 |
| L3 | 4 – 5 | 80 | 2.2 | 0.03 | - | |
| L3 | 5 – 6 | 70 | 2.5 | 0.03 | - | |
| L3 | 6 – 7 | 23 | 3.1 | 0.06 | - | |
| L3 | 7 – 8 | 8 | 3.2 | 0.09 | - | 150 |
| L4 | 4 – 5 | 10 | 3.8 | 0.09 | - | |
| L4 | 5 – 6 | 30 | 4.1 | 0.05 | - | |
| L4 | 6 – 7 | 15 | 5.1 | 0.06 | - | |
| L4 | 7 – 8 | 5 | 6.2 | 0.11 | - | 300 |
| S4 | 4 – 5 | 10 | 3.8 | - | 0.09 | |
| S4 | 5 – 6 | 30 | 4.1 | - | 0.05 | |
| S4 | 6 – 7 | 15 | 5.1 | - | 0.06 | |
| S4 | 7 – 8 | 5 | 6.2 | - | 0.11 | 300 |
| **Total** | | | | | | **900** |

Table 3: Expected statistical uncertainty on $A_{LL}$ and $A_{LS}$ for each of the 22 proposed $s$ bins.

## 4.4 Statistical Uncertainty

The simulated values obtained for the numbers described above can be used to estimate the statistical uncertainty on the polarization observables ($\Delta A_{LL}$ and $\Delta A_{LS}$) according to:

$$\Delta A_{LL} = \frac{1}{\sqrt{\frac{N_{\text{WACS}}}{D} P_p P_\gamma}},$$

where $N_{\text{WACS}}$ is the total number of accumulated WACS events, $P_\gamma$ is the photon beam polarization, $P_p = 0.75$ is the average proton polarization in the target, and $D$ is the background dilution factor. As extracted from Figure 16, the $P_\gamma$ factor for the each 8.8 GeV beam $s$ bin is 0.52, 0.63, 0.72 and 0.77, respectively, and 0.63 and 0.75 for the 11 GeV beam bins.

The statistical uncertainty on the WACS polarisation observables for a given number of beam hours can now be estimated. The beam-time estimate and detailed breakdown is given in Table 3, and is based on the requirement of 10% or better statistical uncertainty in at least one $s$ bin. One can see that the beam-time needed for the measurements at $\theta_p^{\text{cm}} = 110^\circ$ is the most significant as a result of the WACS cross section falling off more rapidly as $-t$ increases than the pion photo-production cross section.

## 4.5 Systematic Uncertainty

| Uncertainty | Systematic [%] |
|---|---|
| Beam polarimetry | 1.0 |
| Target polarimetry | 3.0 |
| Packing fraction | 3.0 |
| Charge determination | 1.0 |
| Trigger/tracking efficiency | 2.0 |
| Acceptance | 2.0 |
| Detector resolution and efficiency | 2.0 |
| Background subtraction | 3.0 |
| **Total** | **6.4** |

Table 4: Estimates of the systematic uncertainty contributions to $A_{LL}$ and $A_{LS}$.

Table 4 shows a list of the uncertainties contributing to the systematic error in $A_{LL}$ and $A_{LS}$. With careful uncertainty minimization in polarization, the relative error in the target polarization can be less than 3.9%, as demonstrated in the recent E08-027/E08-007 experiment [49]. Measurements of less than 2.0% have been achieved in an ideal test setting at

UVA. The electron beam polarization measured by Möller polarimetry will have about 1% uncertainty. The uncertainty in the packing fraction of the ammonia target contributes at a level of 3%. Beam charge calibration and detector efficiencies are expected to be known to better than 2%. Detector resolution and efficiency is also expected to contribute less than 2%. The largest point-to-point uncertainty source is associated with the signal extraction. The systematic error on resolving the Compton signal is dependent on the background produced at that kinematic point. A larger background with smaller signal naturally results in a larger error. By considering a larger than expected background we can estimate the expected systematic error from a plausible analysis. We expect less than a 3% systematic contribution from the background subtraction, which is an estimate directly based on the Monte Carlo studies and is in agreement with a similar study performed for E12-14-003.

Adding in quadrature all the (independent) uncertainty sources listed above, the total systematic uncertainty for this experiment is expected to be about 6%. As the error budget is clearly dominated by polarimetry and background subtraction, time–dependent drifts in these quantities must be kept under control.

# 5 Expected Results and Beam-time Request

Results on the differential cross section for WACS from JLab demonstrate that in both the GPD and SCET theoretical frameworks, the relevant form factors exhibit $s$-independence at fixed $-t$ when all of the Mandelstam variables are greater than 2.5 GeV$^2$. This is strong evidence for dominance of the leading quark mechanism and the applicability of factorization in this and other hard exclusive reactions. This will be tested further up to very large values of $s$ and $-t$ in experiment E12-14-003, for which it was decided that all data would meet the above condition.

The physics impact of results on polarization observables in WACS has been diluted somewhat as a result of low values of $-t$ or $-u$, and it looked as though the same might be true for 12 GeV era experiments. However, with the development of new experimental technique based on a pure photon source and large acceptance detectors, the 22 data points which make up the present proposal all unambiguously meet the wide-angle factorization condition ($s$, $-t$, $-u > 2.5$ GeV$^2$). Moreover, at higher values of incident photon energy target mass corrections become much smaller. It is therefore anticipated that the proposed measurements, together with results from E12-14-003, will offer definitive answers to key questions relating to QCD factorization in hard exclusive processes and the non-perturbative structure of the proton.

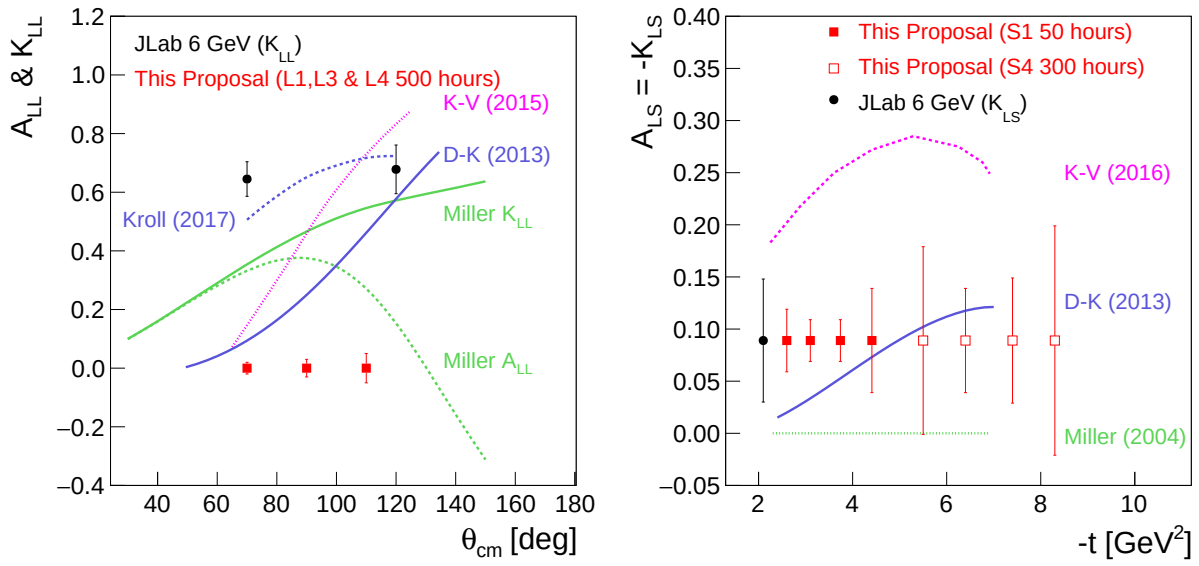


Figure 17: $A_{LL}$ as a function of $\theta_p^{\rm cm}$ (left) and $A_{LS}$ as a function of $-t$ (right), showing the projected impact of the proposed measurement (the left-hand plot shows projections for the $s$-bin with the highest precision for each angle).

## 5.1 Expected Results

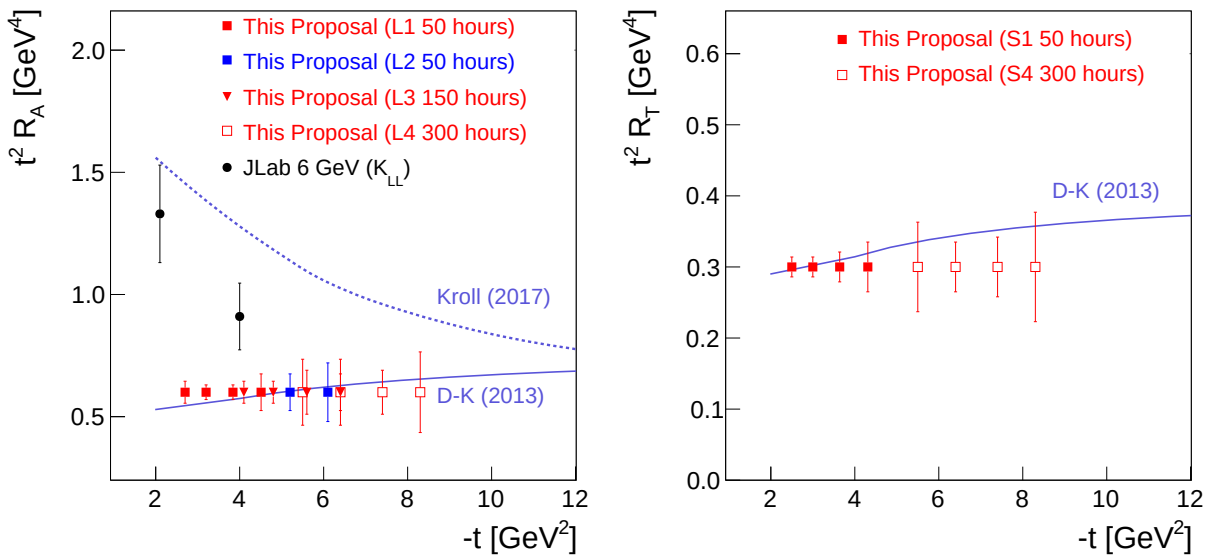


Figure 18: The axial ($R_A$) and tensor ($R_T$) form factors as a function of $-t$, showing the projected impact of the proposed measurement (8.8 GeV red points, 11 GeV blue points).

The priority for the current proposal is the measurement of both $A_{LL}$ and $A_{LS}$ over a broad range of $s$ and $-t$ in the kinematic regime where factorization should be unambiguously applicable. This will provide a natural complement to the differential cross section data which will be obtained in E12-14-003. By comparing the three handbag model predictions for $A_{LL}$ and $A_{LS}$ we can identify unambiguously the reaction mechanism for WACS in this energy regime and test whether it proceeds via the interaction of photons with a current quark or with a constituent quark. The degree to which the dominance of a specific reaction mechanism and the associated applicability of the relevant theoretical approach can be established is shown in Fig. 17, which demonstrates the level of discrimination possible with data for both longitudinal and transverse observables.

Systematic improvements in our knowledge of the relevant non-perturbative matrix elements in these models will be achieved, which is significant as the differential cross section is largely insensitive to those accessible through polarization measurements. In particular, our understanding of the GPDs $\tilde{H}$ and $E$ at high $-t$ will be drastically improved by accurately measuring the form factor ratios $R_A/R_V$ and $R_T/R_V$. This will have a significant and broad impact in the fields of electron and neutrino scattering. The accuracy with which these poorly known, high $-t$ moments of GPDs can be extracted is shown in Fig. 18. Finally, the fact that the data for each kinematic setting will allow for an $s$-scan at fixed $\theta_p^{\rm cm}$ means that an explicit test of factorization can be made. This will also allow verification of the expectation that target mass corrections and higher twist effects are small in this kinematic

regime. Fig. 19 shows the precision with which these fundamental predictions can be tested.

## 5.2 Beam Time Request

| Purpose | Description | Time [h] |
|---|---|---|
| NPS/BigBite calibration | *e-p* elastic | 48 |
| Photon beam and target commissioning | | 24 |
| Packing fraction | Empty and C targets | 34 |
| Möller polarimetry | | 42 |
| Target annealing | | 20 |
| Kinematics change | | 24 |
| BCM/BPM calibration | | 8 |
| Total overhead time | | 200 |
| WACS data production L1 | $A_{LL}$ 8.8 GeV, $\theta_p^{\rm cm} = 70^\circ$ | 50 |
| WACS data production S1 | $A_{LS}$ 8.8 GeV, $\theta_p^{\rm cm} = 70^\circ$ | 50 |
| WACS data production L2 | $A_{LL}$ 11 GeV, $\theta_p^{\rm cm} = 70^\circ$ | 50 |
| WACS data production L3 | $A_{LL}$ 8.8 GeV, $\theta_p^{\rm cm} = 90^\circ$ | 150 |
| WACS data production L4 | $A_{LL}$ 8.8 GeV, $\theta_p^{\rm cm} = 110^\circ$ | 300 |
| WACS data production S4 | $A_{LS}$ 8.8 GeV, $\theta_p^{\rm cm} = 110^\circ$ | 300 |
| **Total** | | **1100** |

Table 5: Beam-time request for the current proposal.

The proposed experiment will use a polarized electron beam of energy 8.8 GeV and 11 GeV with currents of 2.5 $\mu$A. The requested beam time is 1100 hours or 46 days, of which 900 hours are for production running. This is summarized in Table 5.

For each setting, 8 hours will be needed to calibrate the calorimeter with *e-p* elastic coincident events and take BigBite optics data, for which the radiator will be out of the beam line. This leads to a total time for detector calibration of 48 hours. To measure the packing fraction of the material in the target cell, 34 hours in total are needed in order to take empty cell and carbon target measurements. The beam polarization will be measured via Möller polarimetry every time the beam conditions change, which is estimated to be on the order of once every three days. Each measurement will take about 3 hours, leading to a total time for beam polarization of 42 hours.

The target performance is expected to be considerably improved compared to the standard 100 nA electron beam runs. Decay of the target is estimated to be roughly 8 times slower, meaning that annealing of the target will have to be performed much less frequently.

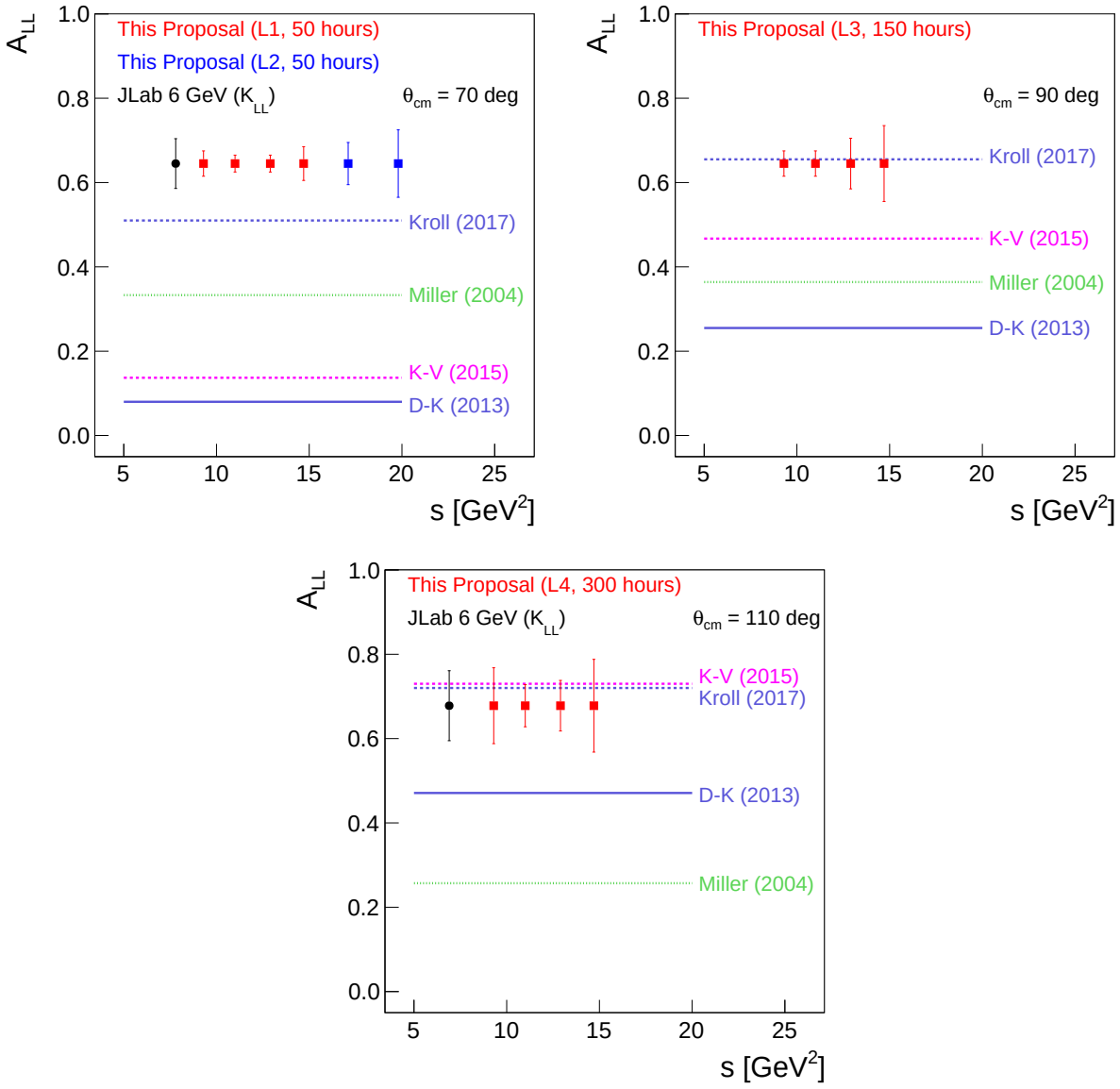


Figure 19: $A_{LL}$ as a function of $s$ at three fixed values of $\theta_p^{\rm cm}$, showing the projected impact of the proposed measurement (8.8 GeV red points, 11 GeV blue points).

It will take about 2 hours to perform one anneal for the target in order to recombine the paramagnetic centers and restore the optimal target polarization. On average, a conservative estimate is that the target will be annealed every 6 days based on estimates that take into account the likelihood of center formation under the high intensity photon source conditions. In total this means 10 anneal periods which results in 20 hours. With this anneal frequency the overall target polarization will be averaging at a higher polarization ($\sim$90%) than previously experiments in Hall A/C ($\sim$70%). It is also expected that a single target load will last for the full experimental run, saving considerable time in pulling and refilling the target cell.

It is estimated that a kinematic setting change (move NPS and BigBite) from point to point will take about 4 hours each, for a total of 24 hours. It is further estimated that 8 hours will be needed to calibrate the BCMs and BPMs and 24 hours committed to commissioning the pure photon beam line.

# 6 Summary

Experiments on Compton scattering in the wide-angle regime have been a part of the nucleon structure program at Jefferson Lab since the early days. Although the total beam-time dedicated to this fundamental reaction has been modest, the results have made a large impact. We anticipate the same will be true for the proposed experiment, and since it is difficult to envisage performing WACS experiments at any future facilities in the medium term, we note that this represents one of the last opportunities to do so.

We request 1100 hours of beam-time to measure the initial state helicity correlation observables $A_{LL}$ and $A_{LS}$ in Wide-angle Compton Scattering (WACS) to an accuracy of 0.1. The experiment will involve scattering circularly polarized photons from a polarized ammonia target at invariant $s$ in the range of 9 to 20 GeV$^2$ for three scattering angles of $\theta_p^{\rm cm} = 70^\circ$, $90^\circ$ and $110^\circ$. The experiment will use 8.8 GeV and 11 GeV, 2.5 $\mu$A, 80% polarized electron beams and a polarized $NH_3$ target. A sweeper–dump magnet combination will be used to produce a narrow, high-intensity photon beam. The scattered photon will be detected by the NPS spectrometer while the BigBite spectrometer will detect the recoil proton.

This combination of a high intensity photon beam and a longitudinal/transverse polarized target will be unique to Jefferson Lab, and will open up the possibility of exploring a range of physics questions that have up to now been inaccessible at tagged photon facilities. Such a program will benefit from the level of expertise within the collaboration on development of new technologies for both polarized targets and large solid angle detectors capable of high rates.

The proposed experiment has a very large figure-of-merit compared to all previous WACS experiments, and each kinematic setting has been carefully chosen in order to reach large $s$ and $t$ in the wide-angle regime and maximize physics impact. These are the optimal conditions for unambiguously testing the applicability of factorization in hard exclusive reactions. The results will have a significant impact beyond the physics of WACS by systematically improving our knowledge of the handbag-based theoretical approaches. This is especially true for the GPDs $E$ and $\tilde{H}$ at high momentum transfer, the latter of which is particularly poorly constrained and will complement data expected at MINERvA.

# References


[1] M.A. Shupe *et al.*, *Phys. Rev.* **D 19**, 1921 (1979).

[2] E.C. Schulte *et al.*, *Phys. Rev. Lett.* **87**, 102302 (2001).

[3] C. Hyde-Wright, A. Nathan, and B. Wojtsekhowski, spokespersons, JLab proposal PR97-108, `https://www.jlab.org/exp_prog/proposals/97/PR97-108.pdf`.

[4] D. Müller *et al.*, *Fortschr. Phys.* **42**, 101 (1994); X.D. Ji, *Phys. Rev. Lett.* **78**, 610 (1997); A.V. Radyushkin, *Phys. Rev.* **D 56**, 5524 (1997).

[5] M. Diehl, T. Feldmann, R. Jakob, P. Kroll, *Eur. Phys. J.* **C 8**, 409 (1999).

[6] C. Hyde-Wright, A. Nathan, and B. Wojtsekhowski, spokespersons, JLab experiment E99-114, `https://www.jlab.org/exp_prog/proposals/99/PR99-114.pdf`.

[7] D. J. Hamilton *et al.*, *Phys. Rev. Lett.* **94**, 242001 (2005).

[8] A. Danagoulian *et al.*, *Phys. Rev. Lett.* **98**, 152001 (2007).

[9] R. Gilman, A. Nathan, and B. Wojtsekhowski, spokespersons, JLab experiment E07-002, `https://www.jlab.org/exp_prog/proposals/07/PR-07-002.pdf`.

[10] C. Fanelli *et al.*, *Phys. Rev. Lett.* **115**, 152001 (2015).

[11] P. Kroll, WUB/17-01 [arXiv:hep-ph/1703.05000v1].

[12] G.A. Miller, *Phys. Rev.* **C 69**, 052201(R) (2004).

[13] D. Day and B. Wojtsekhowski, spokespersons, JLab experiment E05-101, `https://www.jlab.org/exp_prog/proposals/05/PR05-101.pdf`.

[14] D.J. Hamilton, S. Sirca, and B. Wojtsekhowski, spokespersons, JLab experiment E12-14-003, `https://www.jlab.org/exp_prog/proposals/14/PR12-14-003.pdf`.

[15] D. Day, D. Keller, and J. Zhang, spokespersons, JLab experiment E12-14-003, `https://www.jlab.org/exp_prog/proposals/14/PR12-14-006.pdf`.

[16] B. Wojtsekhowski, Super Bigbite Spectrometer, `http://hallaweb.jlab.org/collab/meeting/2009-winter/talks/SBS_project_BW.pdf`.

[17] D. Day, Hall C Meeting, `https://www.jlab.org/Hall-C/talks/01_05_06/Day.pdf`.

[18] J. Zhang, NPS Meeting, `https://wiki.jlab.org/cuawiki/images/9/90/PurePhotonforWACS.pdf`.

[19] B. Wojtsekhowski and G. Niculescu, Technical Note (Conceptual Design Report: A Compact Photon Source), https://wiki.jlab.org/cuawiki/images/d/dd/Concept_Design_Report_Compact_Photon_Source.pdf.

[20] S. Abrahamyan, G. Niculescu, and B. Wojtsekhowski, spokespersons, JLab proposal PR12-15-003, https://www.jlab.org/exp_prog/proposals/15/PR12-15-003.pdf.

[21] D. Day, D. Keller, and J. Zhang, spokespersons, JLab proposal PR12-16-009, https://www.jlab.org/exp_prog/proposals/16/PR12-16-009.pdf.

[22] S. Ali *et al.*, HIPS Workshop 2017 [arXiv:hep-ph/1704.00816].

[23] E. Cisbani *et al.*, Probing transverse nucleon structure at high momentum transfer, http://www.ectstar.eu/node/1656.

[24] S.J. Brodsky and G. Farrar, *Phys. Rev. Lett.* **31**, 1153 (1973).

[25] V.A. Matveev, R.M. Muradyan, and A.V. Tavkheldize, *Lett. Nuovo Cimento* **7**, 719 (1973).

[26] T. Brooks and L. Dixon, *Phys. Rev.* **D 62** 114021 (2000)

[27] C. Bourrely, J. Soffer, Eur. Phys. J. **C 36** 371 (2004)

[28] M. Jones *et al.*, *Phys. Rev. Lett.* **84**, 1398 (2000).

[29] O. Gayou *et al.*, *Phys. Rev. Lett.* **88**, 092301 (2002).

[30] A. Puckett *et al.*, *Phys. Rev. Lett.* **104**, 242301 (2010).

[31] A.V. Radyushkin, *Phys. Rev.* **D 58**, 114008 (1998).

[32] H. W. Huang, P. Kroll, T. Morii, *Eur. Phys. J.* **C 23**, 301 (2002).

[33] X. Ji, *Phys. Rev.* **D 55**, 7114 (1997), *Phys. Rev. Lett.* **78**, 610 (1997).

[34] A.V. Radyushkin, *Phys. Lett.* **B 380**, 417 (1996),

[35] N. Kivel and M. Vanderhaeghen, *Journal of High Energy Physics* **4**, 1 (2013);

[36] N. Kivel and M. Vanderhaeghen, *Nucl. Phys.* **B 883**, 224 (2014); hep-ph/1504.00991 (2015).

[37] M. Diehl, T. Feldmann, R. Jakob and P. Kroll, *Eur. Phys. J.* **C 39**, 1 (2005), arXiv:hep-ph/0408173.

[38] M. Diehl, P. Kroll, *Eur. Phys. J.* **C 73**, 2397 (2013), arXiv:1302.4604.

[39] A.S. Kronfeld and B. Nizic, *Phys. Rev.* **D 44**, 3445 (1991); M. Vanderhaeghen, P.A. M. Guichon and J. Van de Wiele, *Nucl. Phys.* **A 622**, 144c (1997); T. Brooks and L. Dixon, *Phys. Rev.* **D 62** 114021 (2000).

[40] N. Kivel and M. Vanderhaeghen, Nucl. Phys. B883, 224 (2014); arXiv:1504.00991.

[41] N. Kivel, private communication regarding $A_{LS}$ (2016).

[42] G. A. Miller, *Phys. Rev.* **C 66**, 032201 (2002).

[43] D. Pierce *et al.*, Nucl. Inst. and Meth. A 738 154-60 (2014).

[44] Main page of NPS Project,
`http://www.vsl.cua.edu/cua_phy/index.php/MainPage:Nuclear:NPS`

[45] G. Cates, E. Cisbani, G. Franklin, A. Puckett and B. Wojtsekhowski, spokespersons, JLab experiment E12-09-018,
`https://www.jlab.org/exp_prog/proposals/09/PR12-09-018.pdf`.

[46] J.R.M. Annand, B. Quinn, R. Gilman, and B. Wojtsekhowski, spokespersons, JLab experiment E12-09-019,
`https://www.jlab.org/exp_prog/proposals/09/PR12-09-019.pdf`.

[47] K. Gnanvo, Nucl. Inst. and Meth. A 782 77-86 (2015)

[48] S. Abrahamyan and B. Wojtsekhowski, WACS experiment with NPS and SBS,
`https://wiki.jlab.org/cuawiki/images/3/32/Sergey_Abrahamyan_WACS_NPS_2014_update.pdf`.

[49] D. Keller, Nucl. Inst. and Meth. A 728 133-144 (2013)